Meteorol. Atmos. Phys. 78, 261–285 (2001)

Meteorology and Atmospheric Physics

Department of Geophysics and Planetary Sciences, Tel Aviv University, Israel

Synergism of upper-level potential vorticity and mountains in Genoa lee cyclogenesis – A numerical study

M. Tsidulko and **P. Alpert**

With 23 Figures

Received July 31, 2000
Revised June 4, 2001

Summary

The interaction of topography and upper-level potential vorticity (PV) anomaly in intensive case of Alpine lee cyclogenesis (3–6 March 1982) is investigated. The factor separation method is used in conjunction with the PV inversion technique to isolate individual roles of topography and upper-level PV as well as their synergic nonlinear effect. The application of the factor separation method allows to separate low and upper tropospheric dynamics in the real case of lee cyclogenesis and to estimate quantitatively the pure and interactive contributions of topography and upper tropospheric PV anomaly to the pressure deepening in the lee of the Alps.

The PV-topography interactive effect was found to be strong and comparable to the pure PV advection contribution. It is shown that the synergic contribution is responsible for the dipole structure oriented exactly as predicted by theory and as found in the observations. The "pure" topography contribution is small during the "trigger" phase but becomes strongly cyclolytic (i.e., assisting cyclone decay) in the second phase of the lee development. Superposition of the pressure change patterns produced by the two factors along with their interaction, results in a strong deepening in the right location. The joint cyclogenetic action is proposed as the explanation for the fast pressure fall during the "trigger" phase.

1. Introduction

Lee cyclogenesis is a well-known phenomenon in meteorology. The observations show that cyclogenesis occurs to the east of mountains ridges oriented south-north, and to the south of east-west oriented mountains. Taking into account the prevailing direction of air streams in the mountain regions in the world it is possible to identify most cyclogenesis near mountains as "lee" cyclogenesis when it occurs in the lee side of the mountains (e.g., Tibaldi et al., 1990). Though the phenomenon of lee cyclones is well known in synoptic meteorology, the mechanisms responsible for the cyclogenesis in the lee of the mountain ridges have not been clarified for a long time. Currently, there are few mature theories of lee cyclogenesis, and some important features of this phenomenon were already demonstrated, but there is no one uniform theory of lee cyclogenesis. It means that until now there is some lack of agreement about the key dynamic processes contributing to the lee cyclogenesis.

It has been found in several studies that the upper-level dynamics plays a significant role in the process of lee cyclogenesis. Mattocks and Bleck (1986) using idealized numerical simulations for the Alpine cyclogenesis have demonstrated the strong connection between upper-level potential vorticity advection and cyclogenesis in the lee of the mountains. According to their conceptual model, the PV anomaly associated with the advancing jet stream propagates across the mountain ridge while the low-level cold air is blocked by the Alps. The lee cyclone is generated ahead of the PV maximum in the forward left

quadrant of the jet. Mattocks and Bleck (1986) suggested the geostrophic adjustment mechanism as responsible for lee cyclogenesis.

Zupanski and McGinley (1989) also studied the relative roles of topography and upper-level dynamics, but for real data simulations. The importance of upper-level PV advection was again confirmed to be crucial in their experiments. McGinley and Zupanski (1990) investigated more cases for the Alpine cyclogenesis. They studied the roles of upper and lower-level dynamics and found the most powerful lee cyclones depended more on the strength of the upper-level jet, or potential vorticity than on the strength of the lower-level front of baroclinic zone. The front is found to be essential in the cyclone midlife as the intensification takes place.

In a recent paper Egger (1995) studied the interaction of cold air blocking and PV anomaly in upper levels by a two-dimensional model based on the semi-geostrophic equations for three atmospheric layers. The PV anomaly in the upper layer does not determine the circulation in the lowest layer, because the anomaly is above the cold air. In the upper layer the circulation is cyclonic, in the lowest layer it is anticyclonic. The mountain enables the upper-layer PV anomaly to propagate ahead and to outrun the cold air, and since the near-surface cold air has been retarded, a cyclone in the lee side of the ridge is established.

In the present study, we apply the factor separation method (Stein and Alpert, 1993) to the upper-level PV and the mountains in order to estimate their relative roles in real-data simulations of a Genoa cyclone. The most intensive ALPEX case of 3–6 March 1982 was chosen for the simulations. This case seems to be the most studied both observationally (Buzzi et al., 1985; Buzzi et al., 1987) and by numerical simulations (Tafferner and Egger, 1990; Tibaldi and Buzzi, 1983; Bleck and Mattocks, 1984; Dell'Osso, 1984). Our previous simulations of this case are presented in Alpert et al. (1995a, b, c; 1996). Alpert et al. (1996) present a table summarizing earlier studies of this case and their primary focus. The advantage of the factor separation is that it enables the quantitative separation of the synergic interactions. For instance, the joint contribution by the upper-level PV and topographic blocking will be separated here and distinguished from the "pure" contribution due to any of these factors acting alone. None of our earlier studies has separated the upper-level contribution and its synergism with lower-level processes.

There are several problems with the numerical simulations of this case. It was relatively difficult to perform an accurate simulation even with high-resolution mesoscale models. Dell'Osso (1984) discusses problems related to differences between objective and subjective analyses, model resolution and the topographical presentation. The model resolution and accuracy of topography play a crucial role in the simulations. The envelope topography was found to improve the predictions; i.e. increasing the horizontal resolution relaxes the requirement for "envelope" topography.

Here, the NCAR/PSU mesoscale model (MM5) (Grell et al., 1993) is employed for the simulations. For the factor separation experiments, a relatively coarse grid with 90 km resolution and envelope orography is employed. It was found in our earlier simulations that a relatively large domain with such a resolution decreases the lateral boundary effect that was shown to be significant in sensitivity studies of this case (Alpert et al., 1996). Also, the simulation with the same domain and two additional nests with horizontal intervals of 30 km and 10 km yield results, which are in good agreement with observations (Tsidulko, 1998).

In the following section (Sect. 2), we describe the methodology of factor separation for topography and upper-level PV, applied here to the MM5 simulations. The other sections describe the experiments (Sect. 3), their results (Sect. 4) and finally in Sect. 5 the discussion.

2. Methodology

In this section, we shortly describe two tools that were adopted in this study, i.e. the factor separation method and the PV inversion for the MM5 mesoscale fields.

2.1 Factor separation method

The factor separation method was developed by Stein and Alpert (1993, SA hereafter) and in recent years was successfully applied to a number of studies (Alpert and Tsidulko, 1994; Alpert et al., 1995a, b, c, 1996; Khain et al., 1993). The

method allows the calculation of both the ''pure'' and synergic contributions of several factors on a resulting field. Running of factor/no factor simulations is a common approach in numerical modeling. Alpert et al. (1995a) show that the difference between factor/no factor simulations may not actually be the ''true'' impact of that factor, since this difference normally contains also synergic effects of the factor with other factors that were not chosen in the particular experiment. A short description of the method follows.

If we wish to examine two factors, four on/off simulations are required,

$$f_0 = \hat{f}_0, \tag{2.1}$$

$$f_1 = \hat{f}_0 + \hat{f}_1, \tag{2.2}$$

$$f_2 = \hat{f}_0 + \hat{f}_2, \tag{2.3}$$

$$f_{12} = \hat{f}_0 + \hat{f}_1 + \hat{f}_2 + \hat{f}_{12}, \tag{2.4}$$

where f_0, f_1, f_2, f_{12} are the resulting fields in four simulations, and $\hat{f}_0, \hat{f}_1, \hat{f}_2$ are the separated contributions of the so-called ''factor-independent'' (i.e., $\hat{f}_0$) and the two studied factors, respectively. The term $\hat{f}_{12}$ is the synergic contribution of the two factors. The ''factor-independent'' here refers to the contribution (to the field f) when both factors are switched off. In this terminology f_1, for instance, refers to the resulting field when only factor no. 1 is switched on. The ''hat'' function $\hat{f}_1$, for instance, is the resulting ''pure'' contribution by factor no. 1 calculated by the factor separation method as outlined next. These equations yield:

$$\hat{f}_0 = f_0, \tag{2.5}$$

$$\hat{f}_1 = f_1 - f_0, \tag{2.6}$$

$$\hat{f}_2 = f_2 - f_0, \tag{2.7}$$

$$\hat{f}_{12} = f_{12} - (f_1 + f_2) + f_0. \tag{2.8}$$

SA have shown that for estimation of pure and synergic effects of n factors, 2^n simulations are required.

Earlier, we have already applied the factor separation method to the Genoa lee cyclogenesis (Alpert et al., 1995b; 1996). In the first study four factors – topography, latent and sensible heat fluxes and the latent heat release were chosen; in the second study the chosen factors were: topography, lateral boundary and initial conditions. In Alpert et al. (1995a) it was shown that without the factor separation method the impact of one factor could be erroneously associated with another factor due to synergism. If, for instance, we choose latent heat release (i.e., convection) as a factor in our lee cyclogenesis study and make only one pair of factor/no factor simulations, we obtain an artificially large latent heat release impact also at the first stage of lee cyclogenesis, while in reality it is almost entirely expressing the hidden synergic effect of the convection with topography, and *not* the pure contribution of latent heat release.

Here, the factor separation method is further applied to estimate the pure and synergic effects of topography and the upper-level dynamics, or upper-level jet stream. In earlier on/off studies and factor separation applications so far, only topography and diabatic processes were examined. In Alpert et al. (1996) the factor separation method was applied to boundary and initial conditions. The boundary was switched off by updating the lateral boundaries with a linear time interpolation from the beginning to the end of the simulation without using real boundary data during the simulation. The initial conditions were switched off by virtually smoothing the initial fields at all levels.

In the current study the factor separation method is applied to the upper-level dynamics by using the PV-inversion scheme (e.g., Mattocks and Bleck, 1986), which is more accurate, compared to any interpolation and/or smoothing, method. The upper level potential vorticity (PV) field was smoothed in order to estimate the contribution of the jet stream and upper level dynamics. The ''invertibility principle'' (Hoskins et al., 1985) is applied for the calculation of all the initial fields as described in the next section.

2.2 PV inversion of the MM5 fields

The ''invertibility principle'' of potential vorticity was introduced for practical use by Hoskins et al. (1985). The main idea of this principle is that it is possible, with some minimum conditions (as described later), to deduce the complete structure of the large-scale flow using only the 3-D potential vorticity spatial distribution with

boundary conditions. PV is defined in the isentropic-coordinate system as

$$\mathrm{PV}_\theta = -g(f + \mathbf{k} \cdot \nabla_\theta \times \mathbf{V})\left(\frac{\partial p}{\partial \theta}\right)^{-1}, \qquad (2.9)$$

where g is acceleration of gravity, θ – potential temperature, $\mathbf{k}$ is a vertical unit vector, ∇_θ – three-dimensional gradient operator, f – Coriolis parameter, $\mathbf{V}$ – horizontal wind vector and p – pressure. According to the Ertel vorticity theorem PV is conserved for frictionless adiabatic motion. The PV inversion yields the complete field description of pressure, wind and temperature. Few additional conditions must be satisfied. First, a balance condition is needed; the simplest but least accurate option is the geostrophic balance, some reference state should be satisfied and the boundary conditions should be defined.

Recently, piecewise PV inversion was successfully applied in a number of studies. Both quasigeostrophic PV inversion (Robinson, 1988; Black and Dole, 1993; Hakim et al., 1996; Henderson et al., 1999) and a more precise method using the Charney's (1955) nonlinear balance equation (Davis and Emanuel, 1991; Wu and Emanuel, 1993; Huo et al., 1998) were employed. This technique is usually employed for case studies of a variety of cyclones, especially hurricanes. Wu and Emanuel (1993) have utilized the PV diagnostic and inversion in order to isolate the positive PV anomaly of a hurricane and to evaluate the large-scale environmental factors responsible for the cyclone's movement and the storm's influence on its own track. Henderson et al. (1999) apply quasigeostrophic PV inversion to investigate the contribution of different synoptic scale features to the steering flow. Huo et al. (1998) use the PV inversion method in order to improve the model initial conditions. They treat the temperature errors in objective analysis over the ocean as a surrogate PV anomaly. Inverting this PV anomaly they obtain the fields of dynamically consistent errors for the model initial conditions.

In a recent study Huo et al. (1999, parts I and II) apply the piecewise PV inversion method to the numerical simulation of the extremely intensive storm of 10–14 March 1993. They isolate different parts of the PV field at a particular time of the simulation (36 hours) and from each PV pattern they derive its own circulation. From this inverted circulation they estimate the contribution of isolated PV features to the total deepening of the cyclone and they study how the inverted field from each particular PV anomaly influences the other isolated PV structures. Then the authors change the initial conditions of the simulation, removing or doubling the PV peaks associated with the troughs to the north and to the south of the cyclone. Their method allows investigating the role of individual PV structures in the total deepening of the cyclone, but not the isolation of the synergistic effect of two or more PV anomalies. Applying the factor separation method, however, allows the quantitative evaluation of both individual and interactive contributions of different PV anomalies.

Here, the invertibility principle was applied to the initial fields and lateral boundaries in the MM5 simulations. The PV inversion program uses the Montgomery potential

$$M = gz + c_p T, \qquad (2.10)$$

on isentropic θ levels in order to calculate the PV. Here, z – height above surface, c_p – specific heat at constant pressure for dry air, T – temperature. Next, the PV field may be modified either by inserting PV anomalies or conversely, by reducing and/or smoothing any existing anomalies. Then by iterating a number of times the Montgomery field is calculated for the new PV field. Finally, new fields of M and PV are used to deduce the pressure and the geostrophic wind fields. For pressure calculation the hydrostatic equation in the isentropic coordinates is used, i.e.,

$$\frac{\partial M}{\partial \theta} = c_p\left(\frac{p}{p_s}\right)^{R/c_p}, \qquad (2.11)$$

where p is pressure, p_s – surface pressure and R, the ideal gas constant.

For the MM5 data the following procedure is adopted:

- The initial fields on pressure levels are interpolated to isentropic θ levels;
- The Montgomery function on θ levels is calculated using (2.10) for the upper level

and the hydrostatic equation (2.11) for other levels;
- The M field is used as an input for the PV inversion program, which provides the new M field according to the PV change and the new pressure fields on isentropic levels using geostrophic balance (Bleck, 1974; Mattocks and Bleck, 1986);
- The temperature and geopotential fields are interpolated to pressure levels;
- The geostrophic wind is calculated;
- All fields are interpolated to the MM5 σ-levels.

This procedure uses the same principle of adjusting the Montgomery function field to the modified PV field as described in Mattocks and Bleck, but here it is applied to the mesoscale model and uses the real data for the simulations.

3. Experiments

3.1 3–6 March 1982 ALPEX case

The case of 3–6 March 1982 was one of the most intense Genoa cyclones during the Alpine Experiment (ALPEX). Figures 1 and 2 show the ECMWF analyses on 3 March 12 GMT and on 5 March 12 GMT at the surface and 500 hPa, respectively. On 3 March 12 GMT, the 500 hPa field was characterized by a wide trough approaching the continent; at the surface, there was a deep vortex over the Atlantic Ocean, northeast of Scotland. A cold front extended from Europe over the Atlantic. The system moved to the east, and 12 hours later, on 4 March 00 GMT the cold front extended all across Europe. It reached the Alpine mountains on 4 March 12 GMT; an intense upper-level jet oriented over the western Mediterranean in northeasterly direction characterized the upper atmosphere. The lee cyclone started its development on 4 March 12 GMT over the western Mediterranean. At 500 hPa, the trough reached the southwest part of the continent and deepened. The surface front reached the Mediterranean on 5 March 00 GMT while the surface cyclone was deepening intensively between 4 March 12 GMT and 5 March 00 GMT – about 9 hPa in 12 hours according to subjective analysis (Dell'Osso, 1984). During the next twelve hours the pressure fall continued and on 5 March 12 GMT the center of the surface cyclone was located a little northeast of Corsica with a central pressure of 1007 hPa, Fig. 1b. A cutoff low formed also at 500 hPa, Fig. 2b. After 5 March 12 GMT the cyclone moved eastward and quickly decayed. The lowest pressure was 1006.7 hPa according to the ECMWF analysis while the subjective analysis (Dell'Osso, 1984) yields there 1004 hPa.

3.2 The model

Version 2 of the PSU/NCAR mesoscale model (MM5) (Grell et al., 1993) was employed. The model is based on the primitive equations. It uses σ-coordinates (23 vertical levels) and an Arakawa-Lamb B horizontal grid, where velocity variables are staggered with respect to scalars (Arakawa and Lamb, 1977). A second-order centered differencing scheme is used for most equations. A fourth-order scheme is applied only to the diffusion terms. For the temporal finite differencing a second-order leapfrog time-step scheme is used. Several options of the physical parameterizations, e.g. precipitation, cumulus convection, boundary layer, radiation, are available in the MM5 model.

To choose the model domain and resolution for our factor separation experiments, a few preliminary simulations of this case were performed. The model domain had to be relatively large in order to avoid the influence of the lateral boundaries in the ''no topography'' simulations, because the boundaries contain information about the real development. As was already mentioned in the introduction, our previous studies of this case (e.g., Alpert et al., 1996) show that the hidden boundary effect in 'no topography' simulations could be relatively large and it may mask the influence of topography. Also, we need a large domain in order to capture the polar jet. Following these conditions, a number of simulations with/without topography was performed with resolution of 60 and 90 km (among others) as well as different numbers of grid points. As a result, the 90 km simulation with 58×73 grid points was chosen for the factor separation experiments. With the enhanced envelope topography option (e.g., Dell'Osso, 1984) it simulates the lee cyclone in good agreement with the analysis and covers a relatively

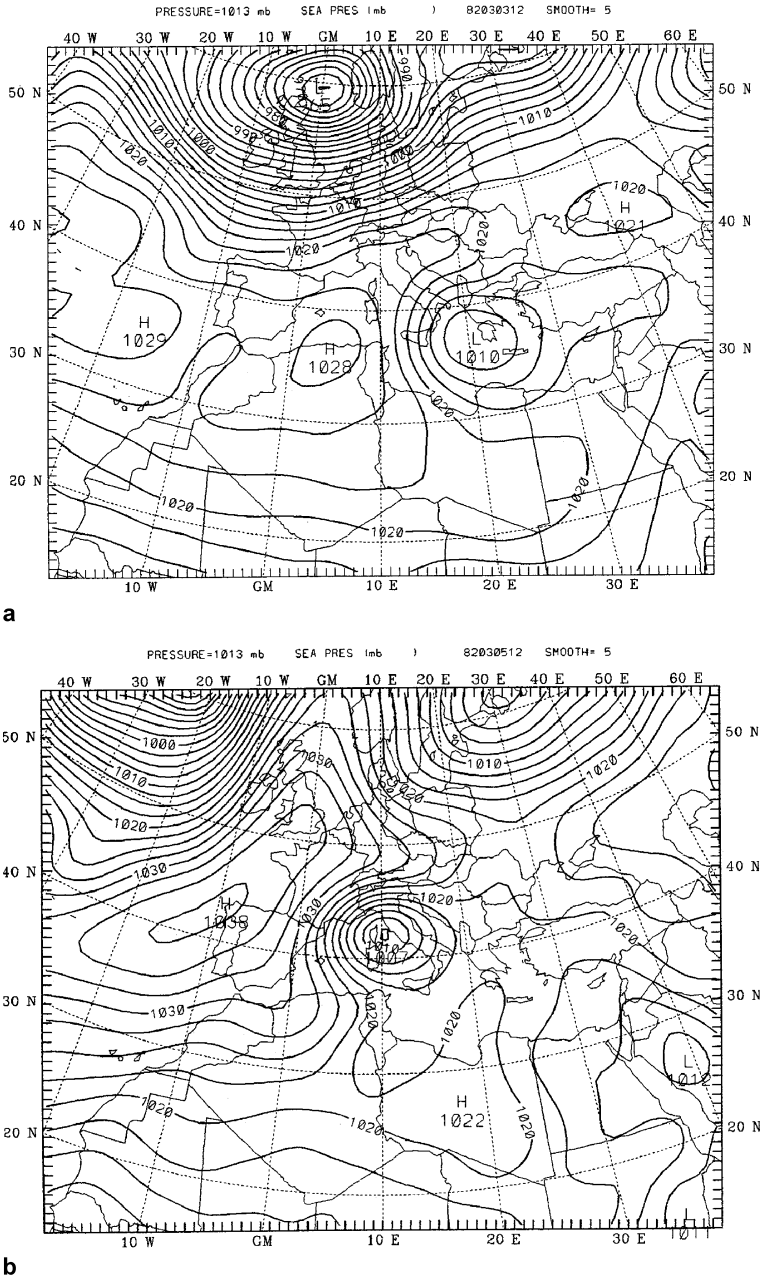

Fig. 1. Sea-level pressure based on ECMWF analyses on the 3–6 March 1982 for the model domain: **a** 3 March 12 GMT; **b** 5 March 12 GMT. Contour interval is 2.5 hPa here and all forthcoming sea-level pressure charts

large domain utilizing reasonable computational effort.

3.3 PV inversion in MM5

The PV inversion procedure as applied to the MM5 model simulations was described earlier in Sect. 2. First, the reference experiment was made. An initial PV field was computed from the initial conditions in this experiment. For the following factor separation experiments, some modification of the initial PV is needed, but first, the PV inversion procedure was applied without PV change, and, for consistency, the initial fields before and after PV inversion were compared. They were found to be similar, but not exactly the same. Except for the accuracy of the PV inversion procedure, the reasons for the small differences are in the interpolation from p-levels to θ-levels and back to p-levels and in smoothing that was applied to the Montgomery potential fields. Also, the wind fields are somewhat different because of the geostrophic relationship assumed in the PV-inversion procedure. Of course, removing of ageostrophic components in the initial conditions will alter the model

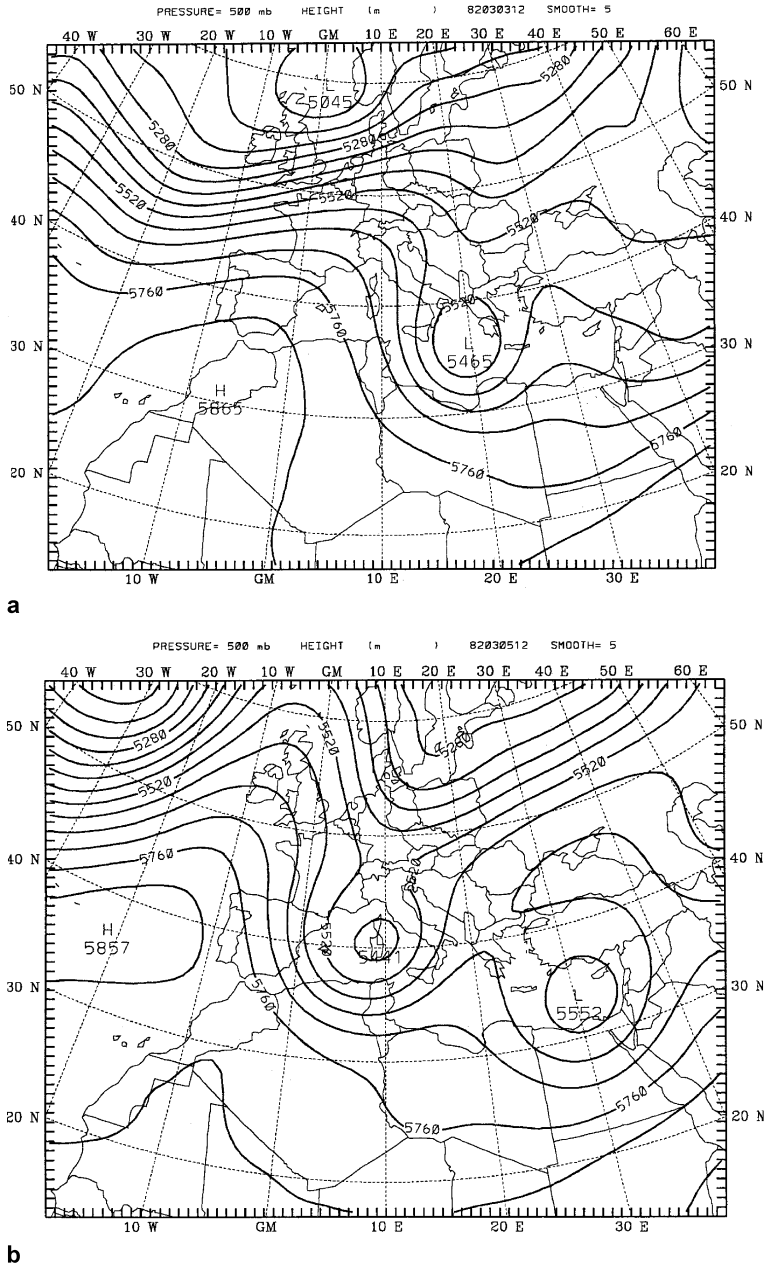

Fig. 2. As Fig. 1, but for 500 hPa geopotential height. Contour interval is 60 m here and all forthcoming 500 hPa charts

during the first few hours, but it doesn't change much the scenario of the simulation, despite the location and the pressure fall are slightly different in cases of ''ageostrophic'' and ''geostrophic'' initial conditions.

This reference experiment, in which the PV-inversion procedure was applied, serves as a ''full control simulation'' in the forthcoming factor separation experiments. The pressure fall in this experiment is in good agreement with the analysis. The location is not very precise, primarily because of the relatively coarse resolution. This small shift in location, however, does not interfere with the forthcoming factor separation for the cyclone development since the reference state is defined by the control experiment.

The aforementioned initial conditions – after PV inversion but without PV change yet – are referred to below as the actual upper-level dynamics with the jet stream, or with PV advection.

Our main purpose in this study is to investigate the interaction of the upper-level dynamics with topography by the factor separation method. To use this method, we need to make a ''no jet'' simulation. Of course, it is impossible to totally ''exclude'' the jet stream and yet not to change

initial conditions in the lower troposphere. So, we tried to weaken the jet by reducing the PV positive anomaly associated with this jet. Hence, the term 'no PV advection' refers to the process of weakening the jet, approaching the Alps. The area of PV alteration was chosen in a way that allowed reduction of both the PV and the jet. For this, the horizontal and vertical distribution of PV anomalies in the initial conditions was examined and the area of maximum PV anomaly was chosen. The horizontal extent of this area is shown in Fig. 3, and in the vertical, the region is located above the 290 K surface (i.e., down to about 500–600 hPa, e.g. Fig. 4). Within this area the PV values were smoothed several hundred times, and then the PV inversion over the whole model domain was applied. The same PV smoothing procedure was also performed on the boundary condition fields. The boundary conditions in our MM5 simulations are extracted from the ECMWF analyses with 12 hours intervals. Since all simulations were for 60 hours, 6 analyses were modified, including the initial one. The first set of ''inverted'' fields served as initial conditions, and from the other five the boundary values were extracted. As seen from Fig. 3a, b

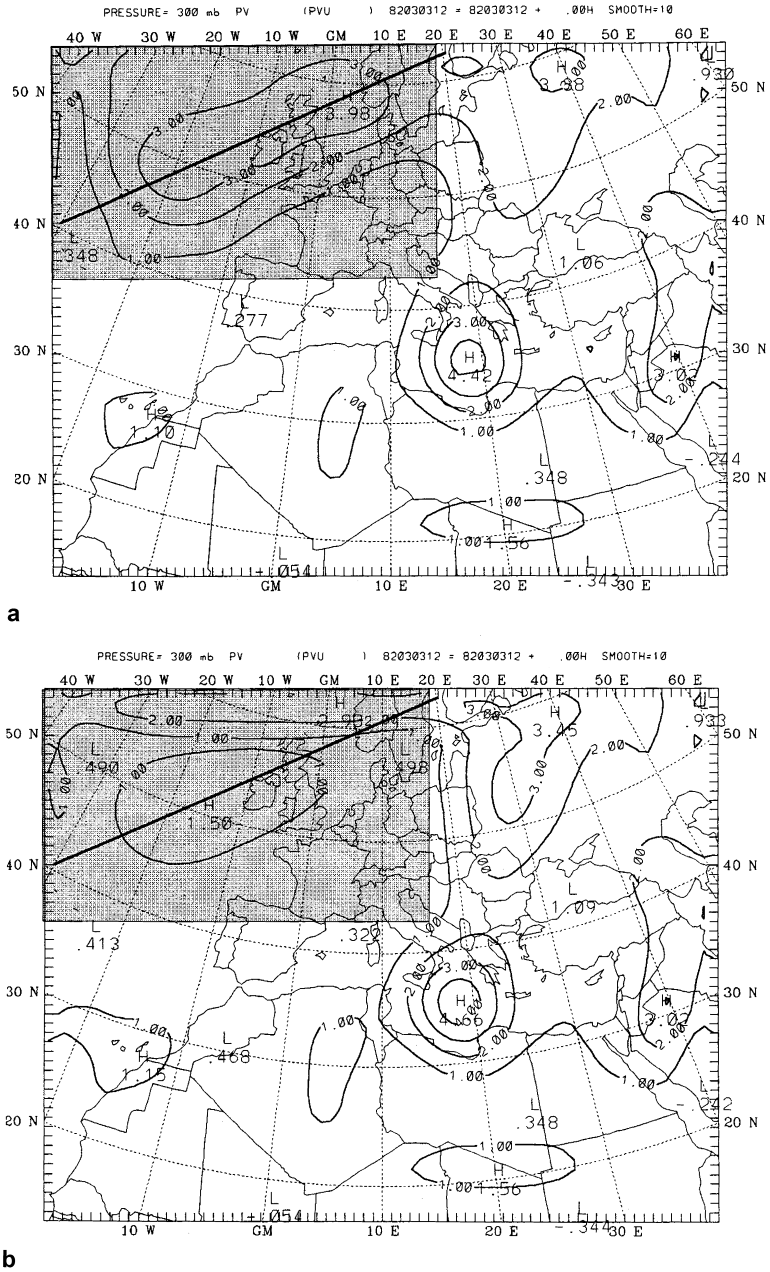

Fig. 3. Initial fields of potential vorticity (in PV units; PVU = 10^{-6} K kg^{-1} m^2 s^{-1}) before **a** and after **b** PV reduction. Contour interval is 1 PVU. The lines indicate the cross-sections shows on Fig. 4. The shaded area indicates the region of PV reduction

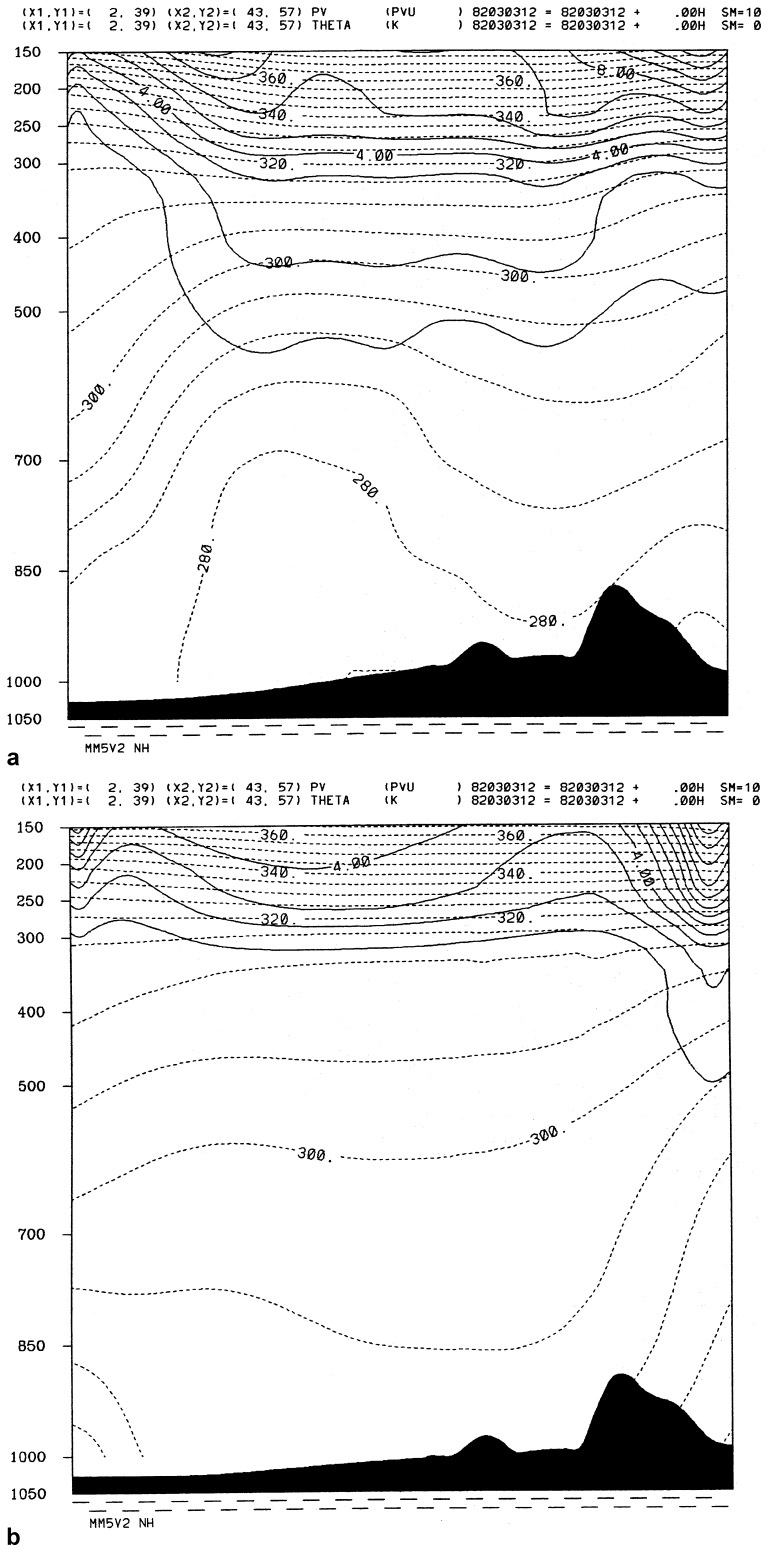

Fig. 4. Initial cross-sections of PV (solid lines) and potential temperature (dashed lines) along the lines indicated on Fig. 3 before **a** and after **b** PV reduction

the PV field is effectively reduced by about a factor of 3, i.e. a PV maximum of 3.98 (Fig. 3a) dropped to 1.50 (Fig. 3b) after smoothing. Of course, the upper-level PV smoothing leads to significant reduction of baroclinicity and frontal strength in the lower atmosphere. It is known that the surface front is a significant factor in lee cyclogenesis, but in the present study we don't try to isolate its influence by factor separation method. Its effect is distributed between pure

and interactive contributions of the factors we are investigating here, i.e. ''large scale'' synoptic, upper-level PV advection and mountains.

Figures 3 and 4 show both PV fields at the 300 hPa level and their cross-sections along the line indicated on Fig. 3 within the marked region. Both the horizontal and vertical slices show a significant reduction of PV in the area of the advancing jet stream, which is equivalent to a ''no jet'' development in the factor separation terminology.

The sea-level pressure initial fields for the ''PV'' and the ''no PV'' simulations are shown in Fig. 5. They are not the same, because PV changes in the upper atmosphere are also reflected at the surface, but these differences are most noticeable in the reduction of the intensity of the 971 hPa cyclone northeast of the British Isles (Fig. 5a). When we reduce the upper-tropospheric PV we increase the amount of mass in the atmospheric column, and this results in increased sea-level pressure over the

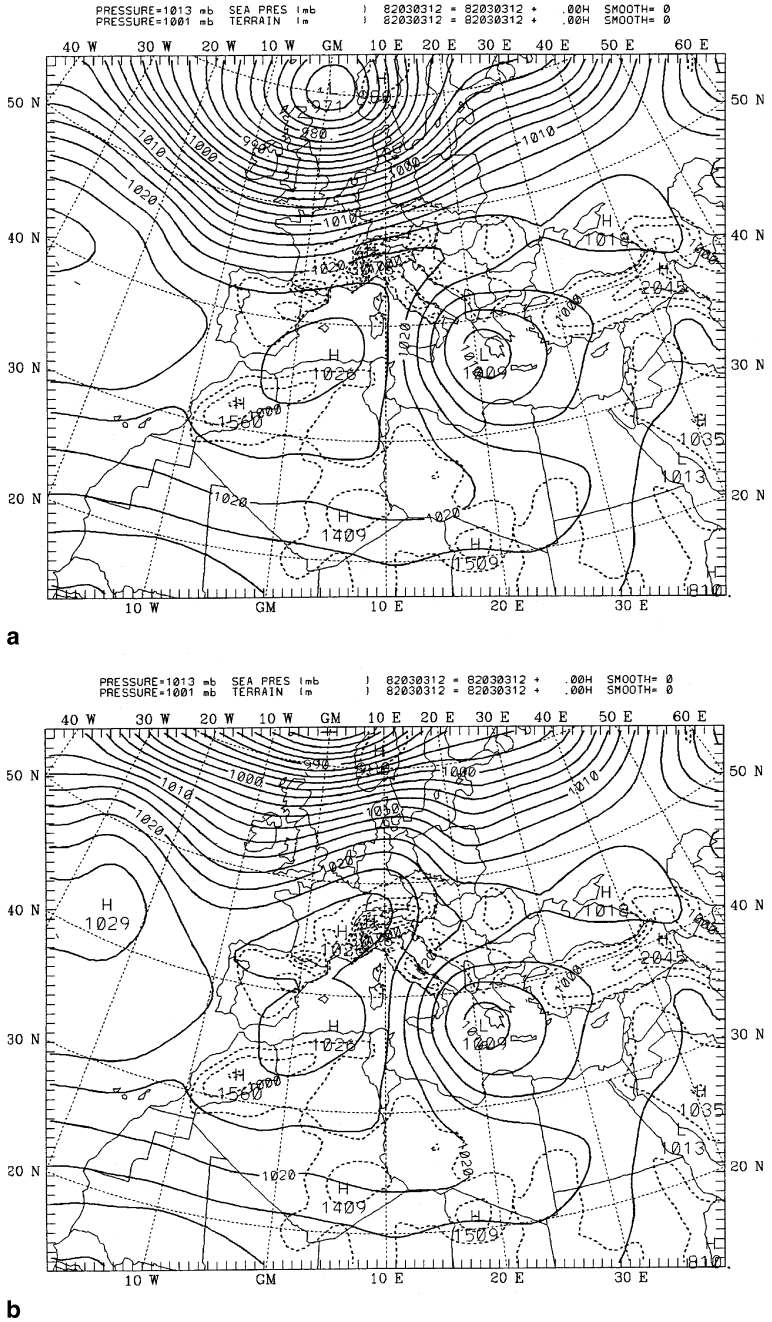

Fig. 5. Initial sea-level pressure fields in experiments with unchanged PV **a**, and modified PV **b**

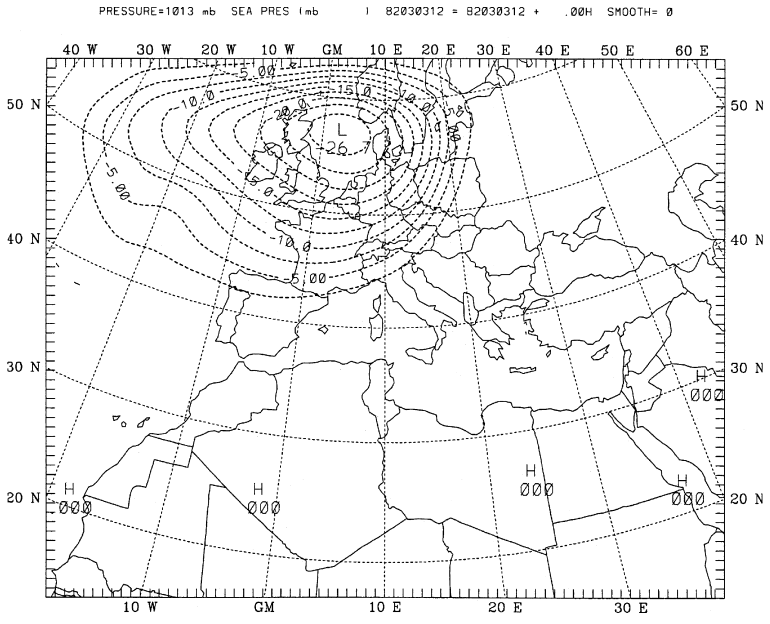

Fig. 6. Sea-level pressure difference (hPa) in initial conditions for experiments with unchanged PV and modified PV

large area of PV modification. Again, the purpose of factor separation experiments is to isolate lower and upper tropospheric dynamics, i.e. to ''remove'' the jet stream flow across the mountains without significant changes in sea level pressure. Since such a goal is impossible to reach in an absolute manner, we can only approximate this ''total'' separation between low and upper tropospheric dynamics. Figure 6 shows the difference in sea level pressure between ''PV+'' and ''PV−'' experiments. It shows that the maximum of this difference (located northeast of British Isles) is significant – about −27 hPa, and is clearly associated with the jet displacement. Over the Alps the differences are not too large. Figure 5 demonstrates that the initial sea level pressure fields for ''PV+'' and ''PV−'' simulations are relatively similar. Also, it is evident from Fig. 6 (and later, from Fig. 22) that in the lee of the Alps the differences in initial sea-level pressure are less than about 2 hPa. It should be noticed that inserting additional mass over the area north of the Alps influences the low-level dynamics. The main feature of the low troposphere, essential for the lee cyclogenesis process, is the cold front, associated with the trough to the north of the Alps and approaching the mountains after about 24 hours of simulation. This feature can be seen in all forthcoming simulations, both with unmodified and reduced upper tropospheric PV anomaly (Figs. 7a, 8a, 9a, 10a).

As required by the factor separation method, four experiments were performed, as follows: with PV and with mountains (PV+TOPO+); with PV and without mountains (PV+TOPO−); without PV and with mountains (PV−TOPO+); without PV and without mountains (PV−TOPO−). In our further discussion, all experiments with reduced PV, i.e. with a weakened jet, are referred to as 'PV−' simulations, while unmodified PV experiments are entitled in short as 'PV+'.

3.4 PV + TOPO + experiment

This simulation is the ''full'' model run and is quite successful in describing the actual development of the cyclone. Indeed, at 24 hours of simulation there is a trough in the lee, slightly modified by the Alps (Fig. 7a); at 36 hours of simulation there is already a closed low with a pressure minimum in good agreement with the analysis – 1011 hPa versus analyzed 1012 hPa (Fig. 7b). At 48 hours of simulation, a deep cyclone has formed at the lee of the Alps with a central value of 1008 hPa compared to 1007 hPa

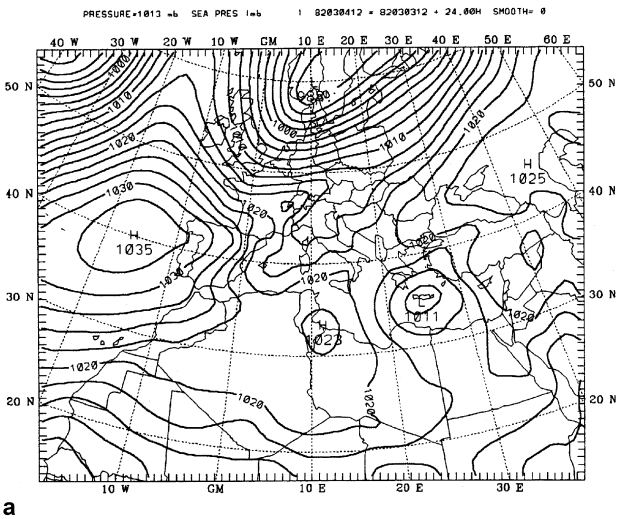

a

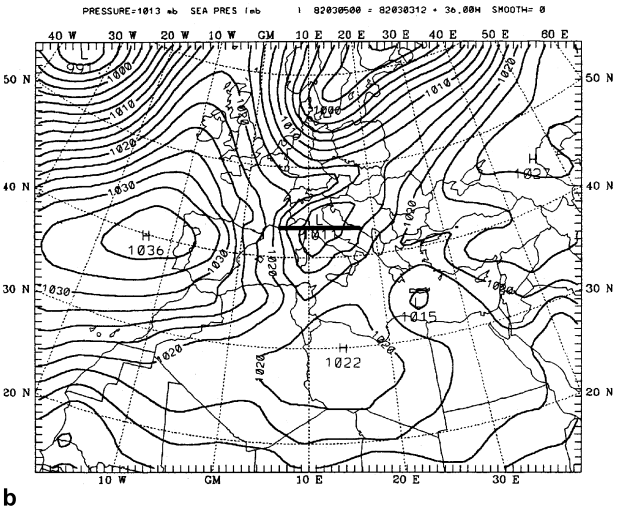

b

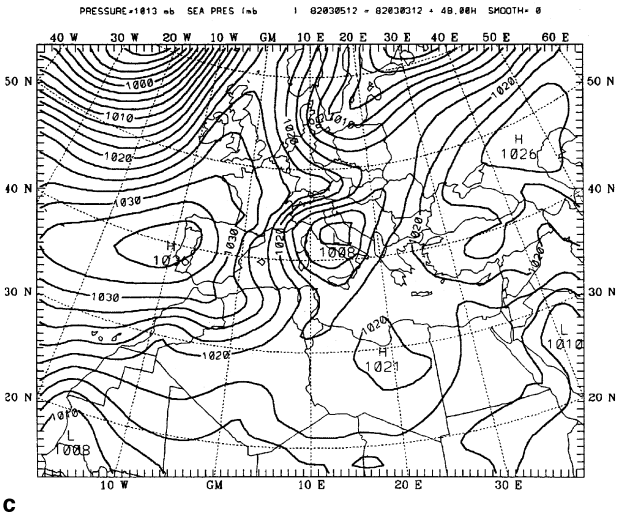

c

Fig. 7. Sea-level pressure at 24 hours (4 March 12 GMT) **a**, 36 hours (5 March 00 GMT), **b** and 48 hours (5 March 12 GMT), **c** of simulation in the *PV+TOPO+* experiment (both PV and topography are switched on, see text). The line on Fig. 7b indicates the cross-section shown on Fig. 17a

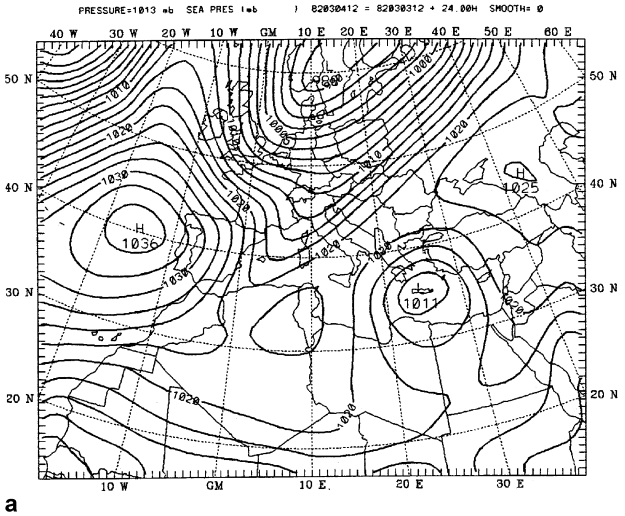

a

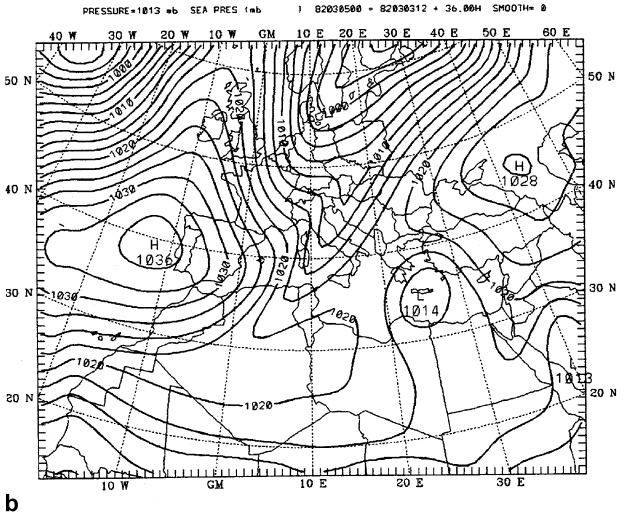

b

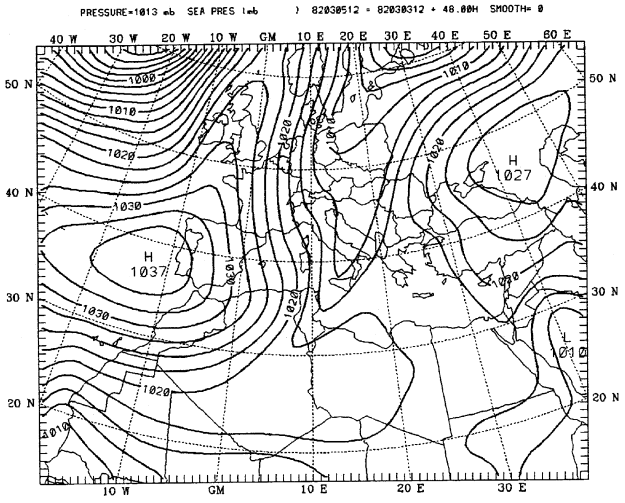

c

Fig. 8. As Fig. 7, but for the *PV+TOPO−* experiment

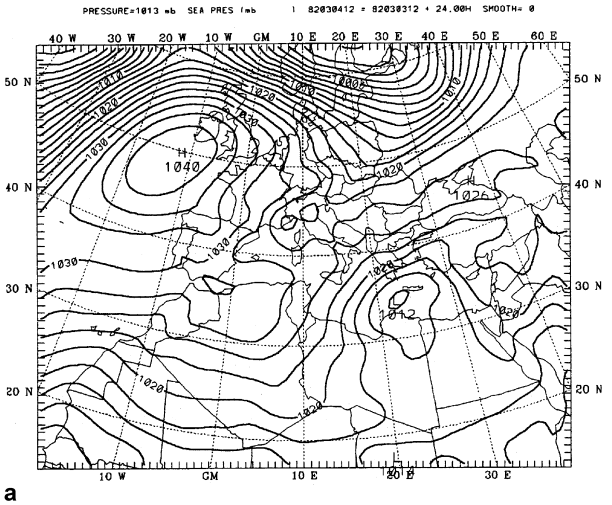

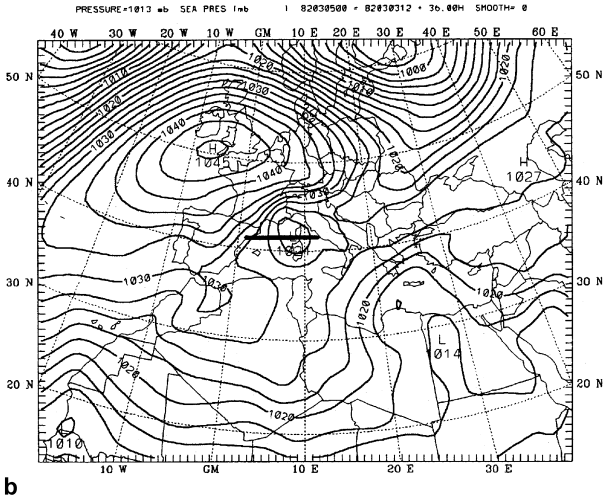

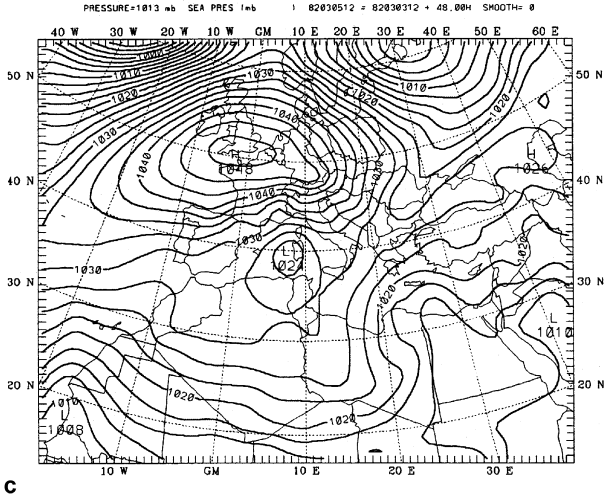

Fig. 9. As Fig. 7, but for the *PV−TOPO+* experiment. The line on Fig. 9b indicates the cross-section shown on Fig. 17b

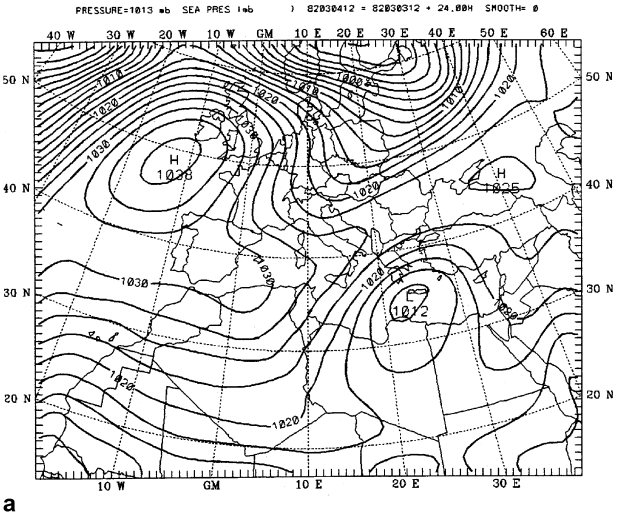

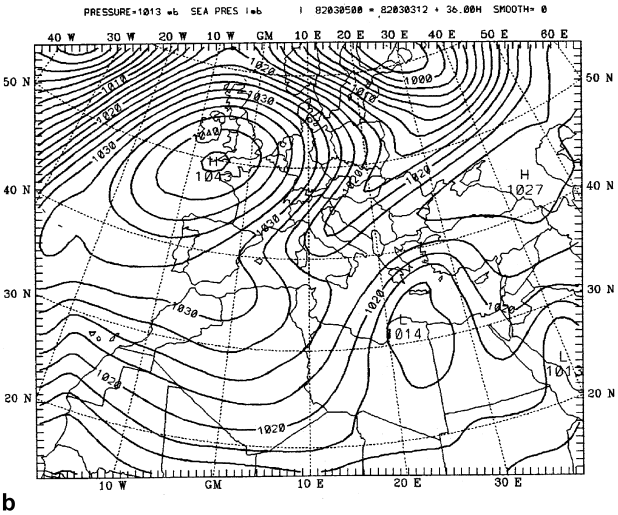

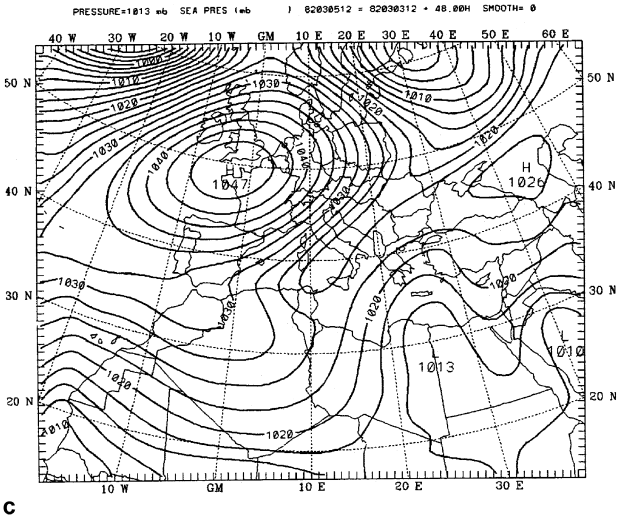

Fig. 10. As Fig. 7, but for the *PV−TOPO−* experiment

in the analysis (Fig. 7c compared to Fig. 1b). Also, the location of the anticyclone west – northwest of Spain is successfully simulated.

Figure 11 presents the 500 hPa heights and winds throughout this "full" simulation. The upper-level trough, associated with the polar jet,

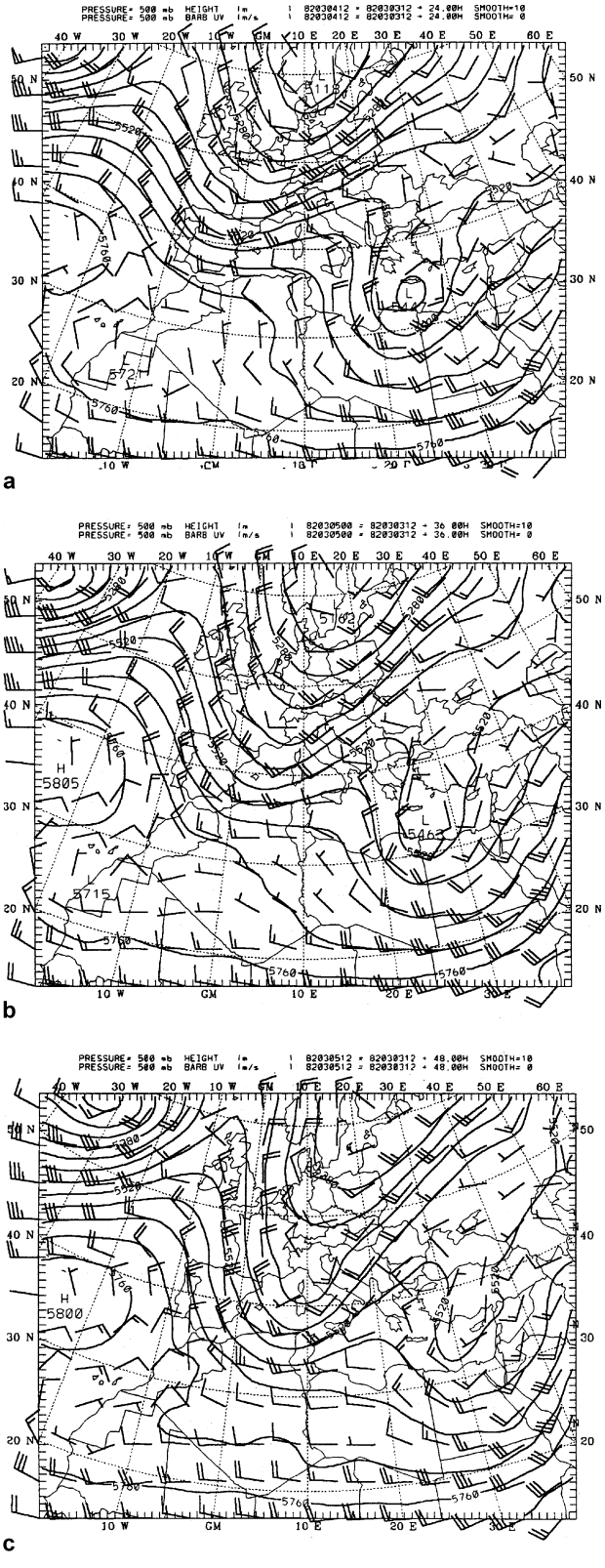

Fig. 11. 500 hPa geopotential height (m) and winds at 24 hours (4 March 12 GMT) **a**, 36 hours (5 March 00 GMT), **b** and 48 hours (5 March 12 GMT), **c** of simulation in the *PV+TOPO+* experiment

approaches the region of the Alps at 24 hours of simulation (Fig. 11a). Then the trough deepens (Fig. 11b), and at 48 hours of simulation the cyclonic circulation is established over the lee region. It should be mentioned that there is no closed isoline, as in the analysis (Fig. 2b). This underestimation of the 500 hPa circulation in the model may be related to our initializing the model not with the actual analysis, but after the PV inversion procedure, even in the "PV+" experiment.

The process of jet propagation to the Alps associated with the PV advection is demonstrated in Fig. 14. During the simulation the jet is moving southward (Fig. 14a), splits into two maxima (Fig. 14b), and forms one separate jet streak in the area of the lee cyclone. A PV peak of 4.4 PVU is established (Fig. 14c).

3.5 PV+TOPO− experiment

This experiment is similar to common simulations "without topography". That means that over the whole model domain the orography is set to be flat (but land-sea distribution is kept as in the full run). The surface trough passes the region without the Alps obstacle; at 24 hours (Fig. 8a) the values in the "lee" are almost the same as in Fig. 7a and the field to the north of the Alps is unmodified; at 36 hours (Fig. 8b) the trough is deepening and there is no closed low, and at 48 hours (Fig. 8c) the trough continues to move in northeasterly direction without any formation of a secondary cyclone in the lee of the Alps.

Differences in 500 hPa height and winds between PV+TOPO+ and PV+TOPO− experiments exist, though they are not as large as in the sea level pressure. The maps at 24 hours seem to be almost the same (Figs. 11a and 12a), but already at 36 hours (Fig. 12b) the trough is narrower, and there is no indication of a closed cyclonic circulation over the area of the Alps at 48 hours of simulation (Fig. 12c). At 300 hPa (Figs. 14, 15) we also see differences between PV+TOPO+ and PV+TOPO− simulations, but the changes are small. The main dissimilarity in these two runs is that the jet is not split into two parts in the PV+TOPO− simulation (Fig. 15b, c).

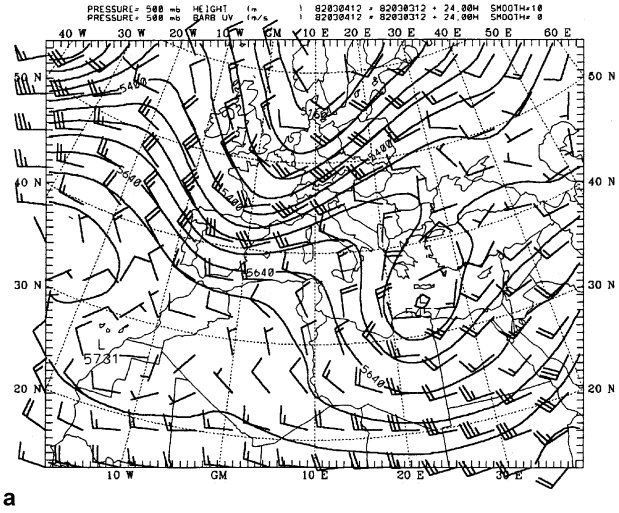

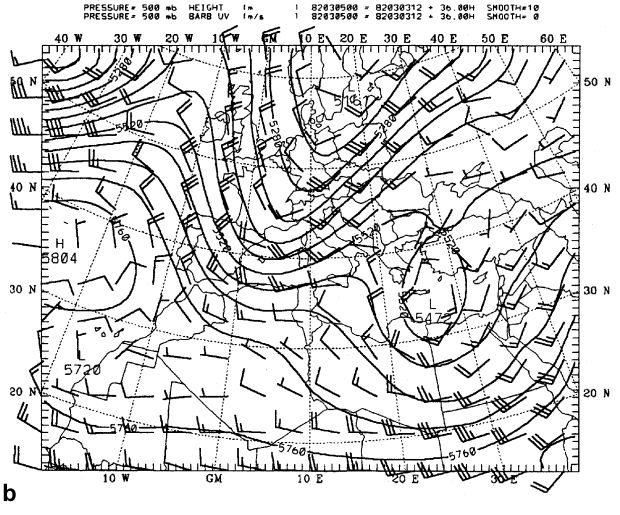

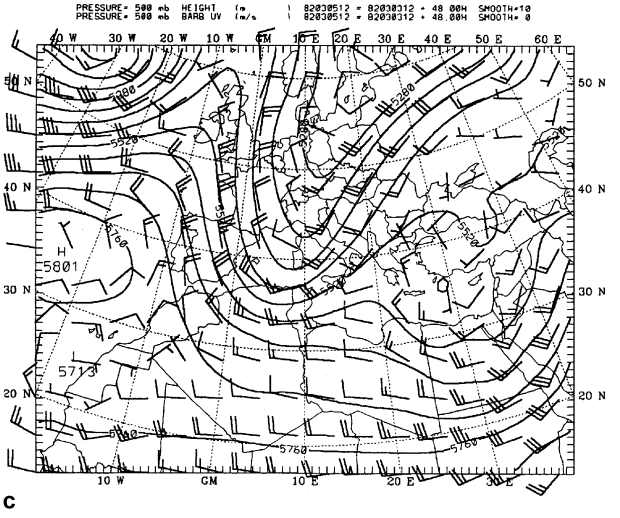

Fig. 12. As Fig. 11, but for the *PV+TOPO−* experiment

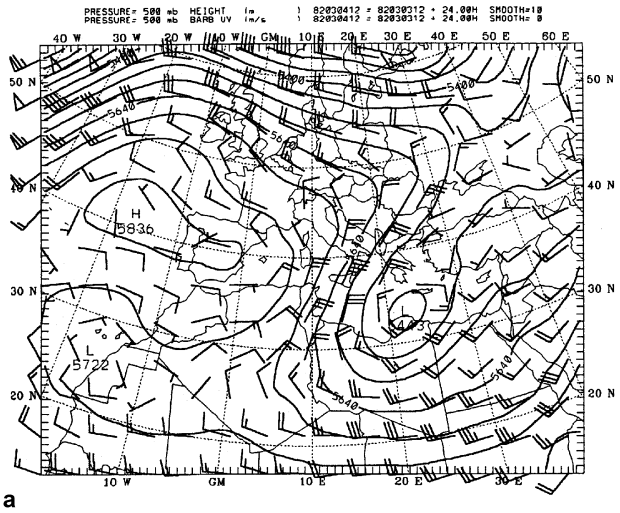

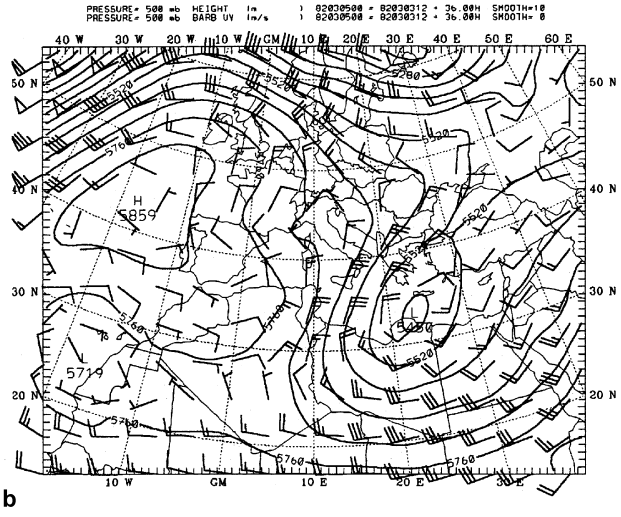

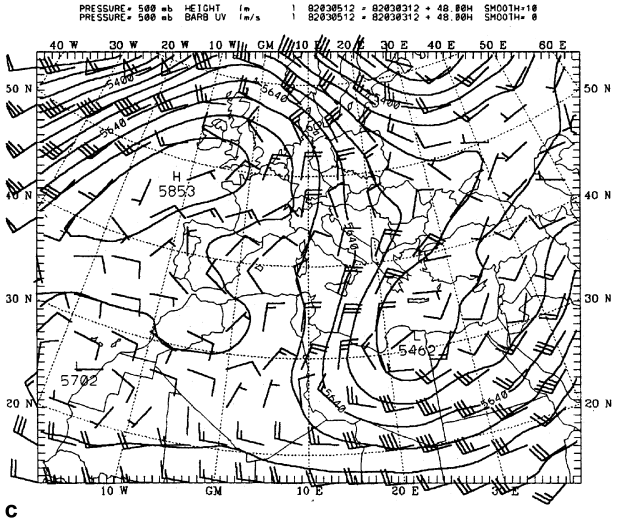

Fig. 13. As Fig. 11, but for the *PV−TOPO+* experiment

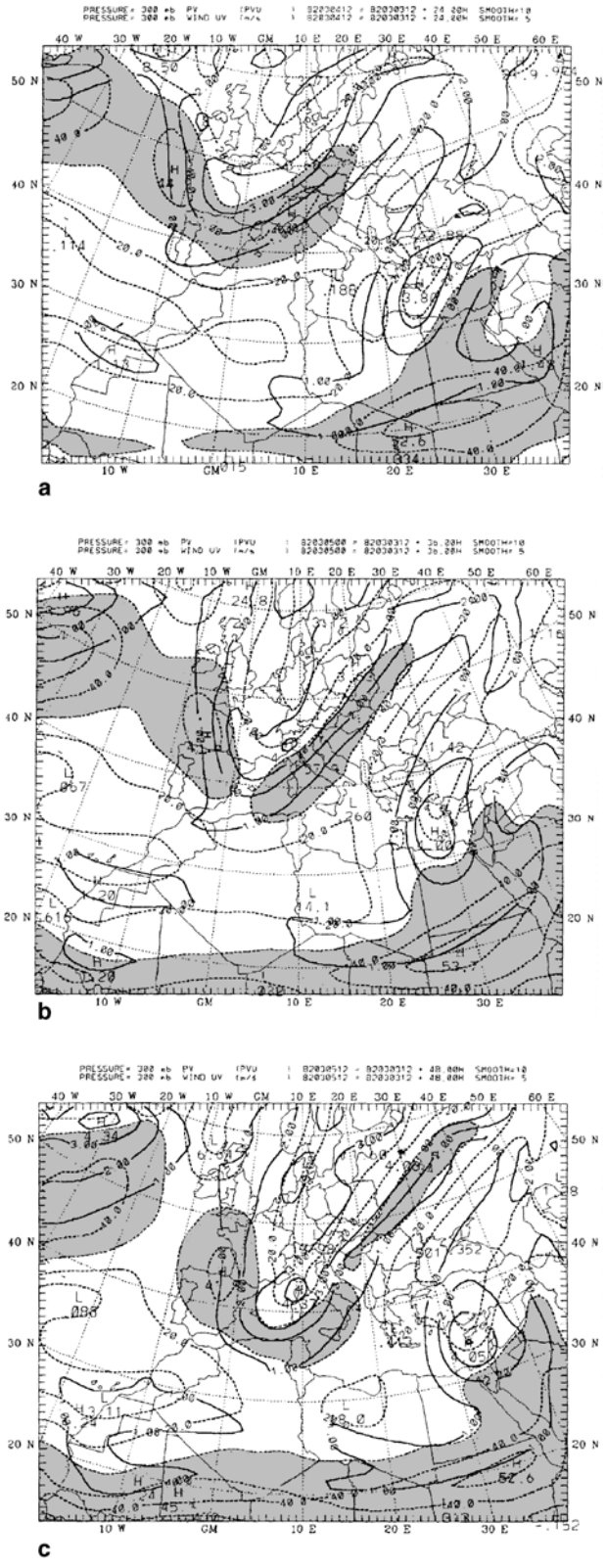

Fig. 14. 300 hPa potential vorticity (solid lines, PV units) and wind (dashed lines, m/s) at 24 hours (4 March 12 GMT) **a**, 36 hours (5 March 00 GMT), **b** and 48 hours (5 March 12 GMT), **c** of simulation in the *PV+TOPO+* experiment. Winds above 30 m/s are shaded

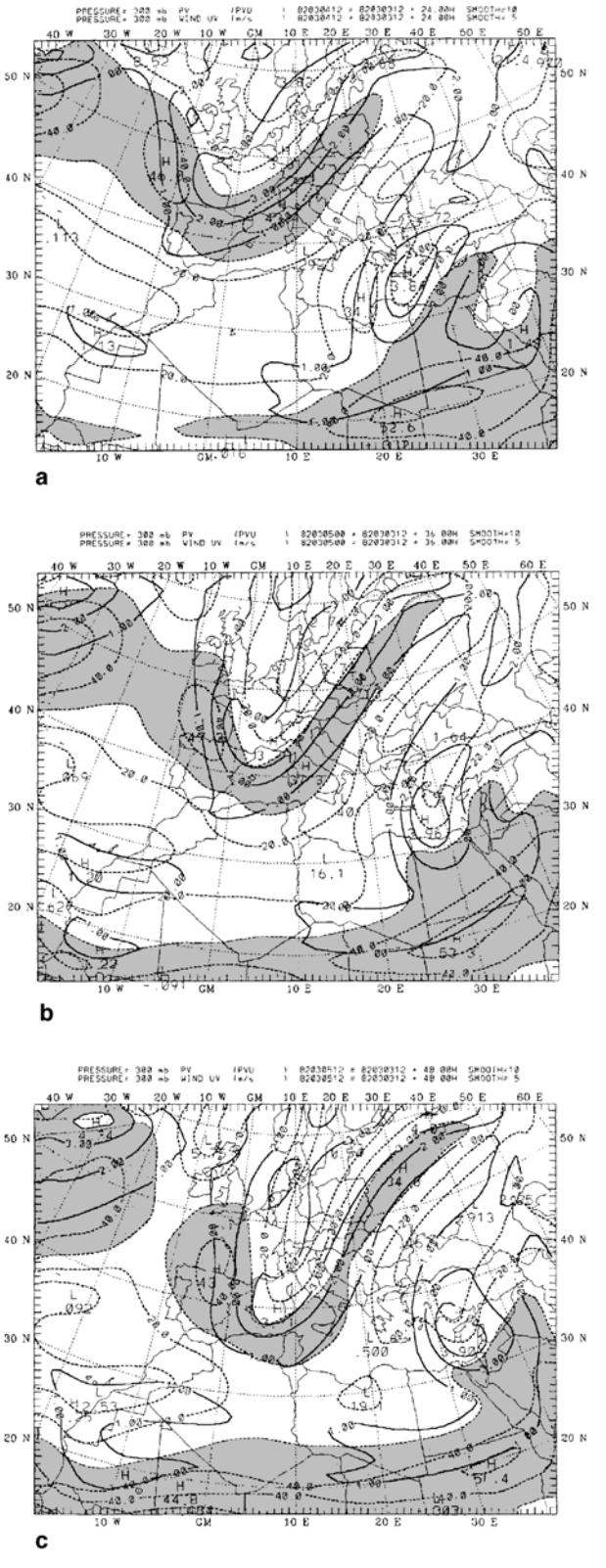

Fig. 15. As Fig. 14, but for the *PV+TOPO−* experiment

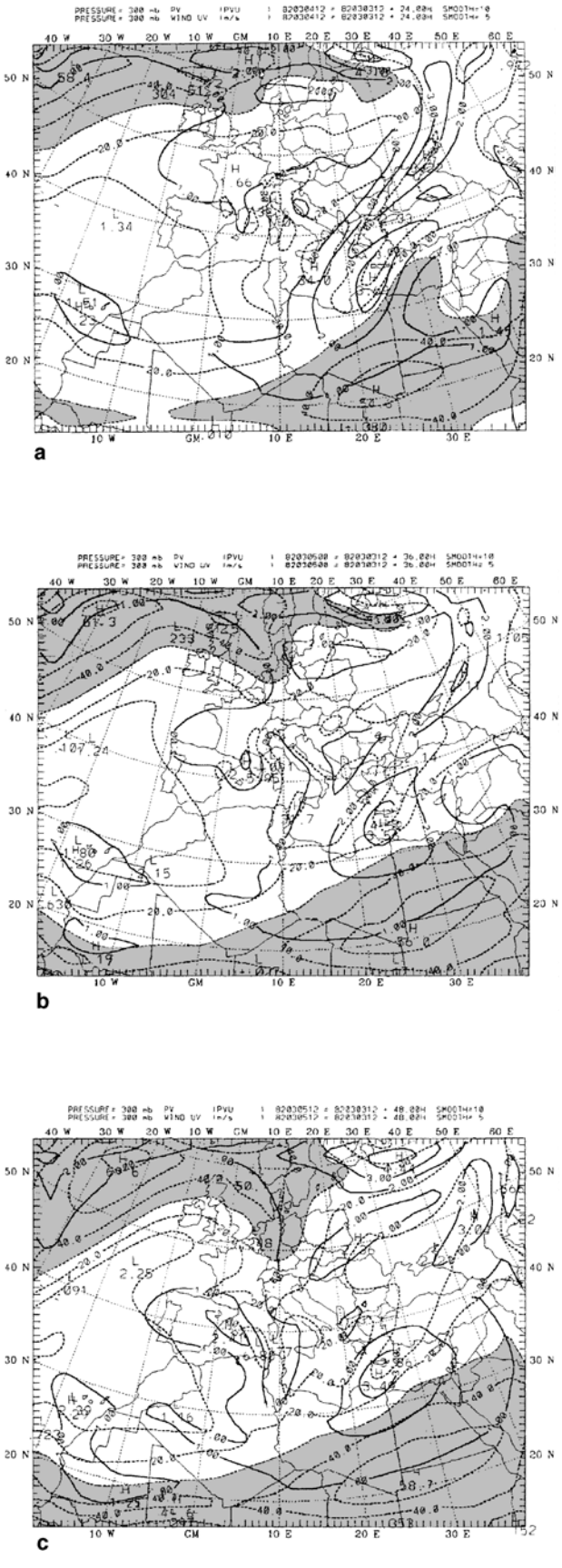

Fig. 16. As Fig. 14, but for the *PV−TOPO+* experiment

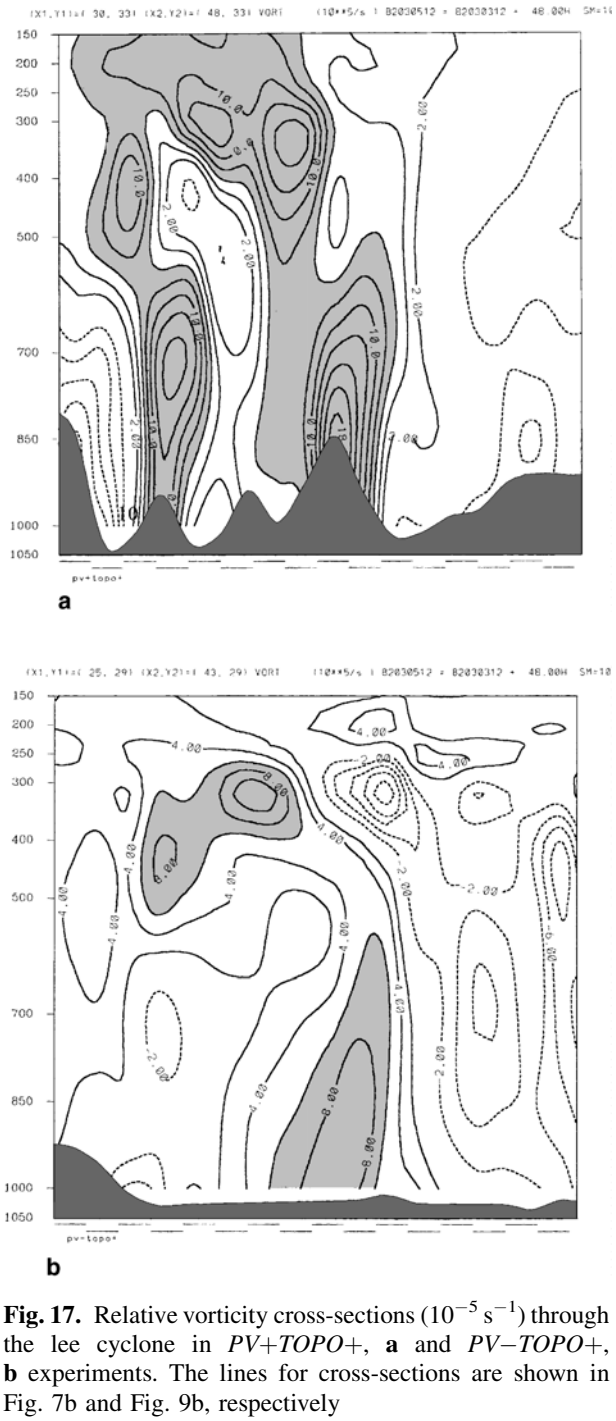

Fig. 17. Relative vorticity cross-sections (10^{-5} s^{-1}) through the lee cyclone in *PV+TOPO+*, **a** and *PV−TOPO+*, **b** experiments. The lines for cross-sections are shown in Fig. 7b and Fig. 9b, respectively

3.6 PV−TOPO+ experiment

The main result of PV−TOPO+ experiment is that we still simulate a cyclone in the lee of the mountains, but it is weaker than in the PV+TOPO+ run. At 24 hours (Fig. 9a) there is the closed low in the lee, and the structure of the pressure field is similar to PV+TOPO+ experiment. At 36 hours a cyclone is formed slightly

to the west from its actual location (Fig. 9b). At 36–48 hours of simulation the lee cyclone moves in southwest direction (Fig. 9c) and begins to fill. A prominent dipole structure is apparent in this simulation; it is even stronger than in the control PV+TOPO+ simulation.

Still, because of PV reduction and propagating differences from the north, the sea-level pressure in the lee might have some bias in the "PV−" simulations, despite the fact that initial differences in the lee are small. In order to evaluate the strength of the cyclonic circulation in PV−TOPO+ experiment, we show some vorticity cross-sections for the PV+TOPO+ and PV−TOPO+ simulations (Fig. 17). The location of the cross-sections is indicated on Figs. 7b and 9b, respectively. The cross-sections show that while in the PV+TOPO+ simulation strong positive vorticity is found throughout the troposphere, in the PV−TOPO+ experiment large values of vorticity exist only below 700 hPa, so the cyclone is significantly diminished in its intensity. It should be noticed that the shallowness of the cyclone might be related also to how the PV smoothing reduces the frontal depth.

The 500 hPa maps (Fig. 13a–c) show that there is no trough or "primary cyclone" approaching the Alps. Strong winds are located much farther to the north and do not reach the mountainous region. We already have seen in the vorticity cross-sections (Fig. 17) that the cyclone in the PV−TOPO+ simulation is relatively shallow, and we do not see cyclonic circulation in the upper troposphere. The same information could be derived from 300 hPa maps (Fig. 16). We clearly see here that the jet does not propagate

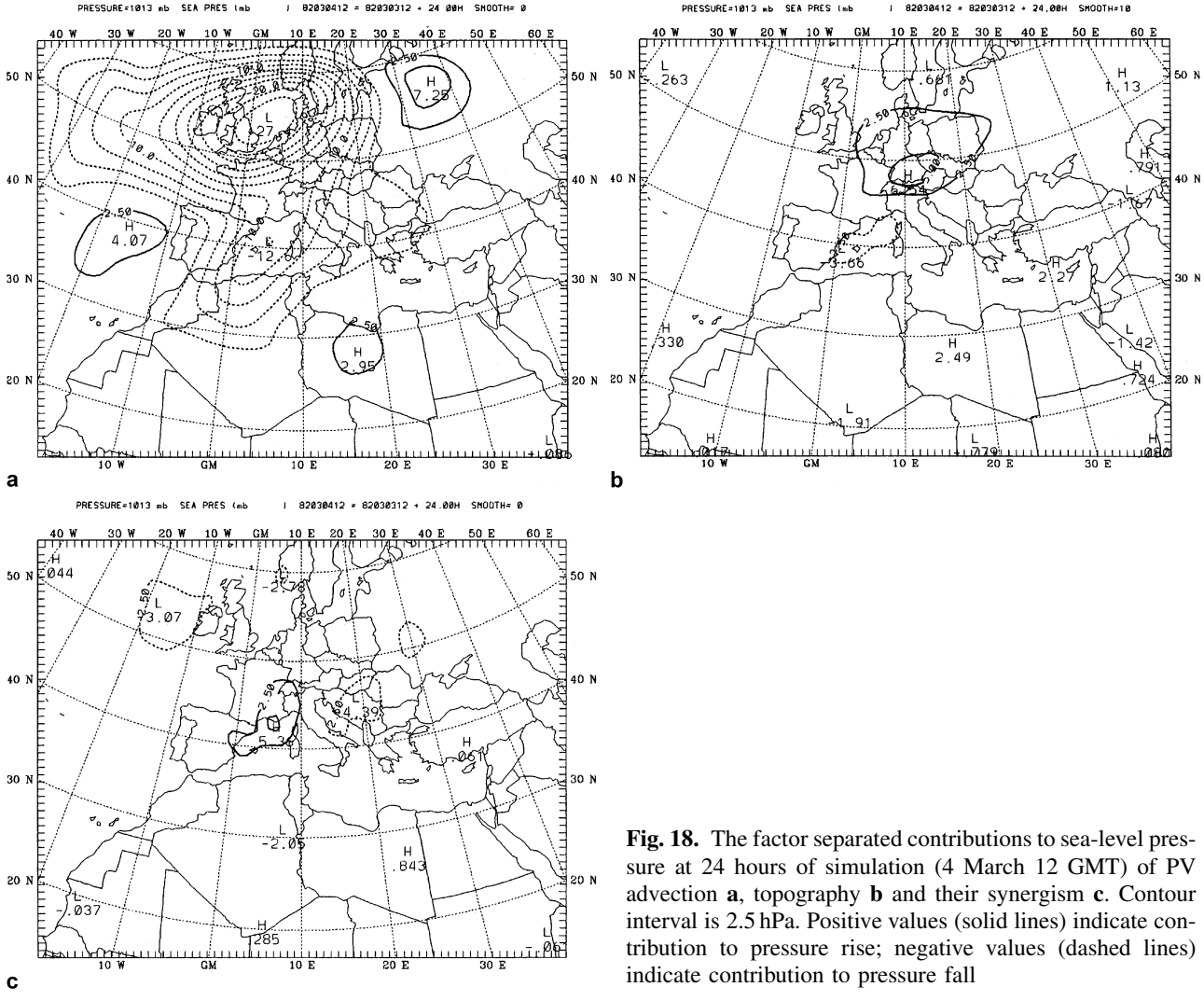

Fig. 18. The factor separated contributions to sea-level pressure at 24 hours of simulation (4 March 12 GMT) of PV advection **a**, topography **b** and their synergism **c**. Contour interval is 2.5 hPa. Positive values (solid lines) indicate contribution to pressure rise; negative values (dashed lines) indicate contribution to pressure fall

southward, and the picture is almost the same throughout the simulation.

3.7 PV−TOPO− experiment

At 24 hours (Fig. 10a) the trough moves slightly northward to its location in the "PV+" simulations. Despite this evolution, at 36 hours and 48 hours the trough is in a similar location to that in PV+TOPO− experiment (Fig. 8b, c), but its orientation is quite different.

Because the cyclone in the PV−TOPO + simulation is relatively weak, the upper-level maps for PV−TOPO− experiment are very similar to the PV−TOPO+ simulation (not shown).

4. Results of the factor separation

In these factor separation experiments mountains were treated as factor number 1, and PV as factor number 2. Following the factor separation notation, the aforementioned simulations are therefore,

$$f_0 = pv - topo-, \tag{4.1}$$

$$f_1 = pv - topo+, \tag{4.2}$$

$$f_2 = pv + topo-, \tag{4.3}$$

$$f_{12} = pv + topo+. \tag{4.4}$$

The factors decomposition as described in Sect. 2 will now be carried out for the sea-level pressure.

4.1 Spatial variation of the factor-separated contributors

Figures 18–20 show the effects of PV (a), topography (b) and their interaction (c) for 24, 36 and 48 hours of simulation, respectively.

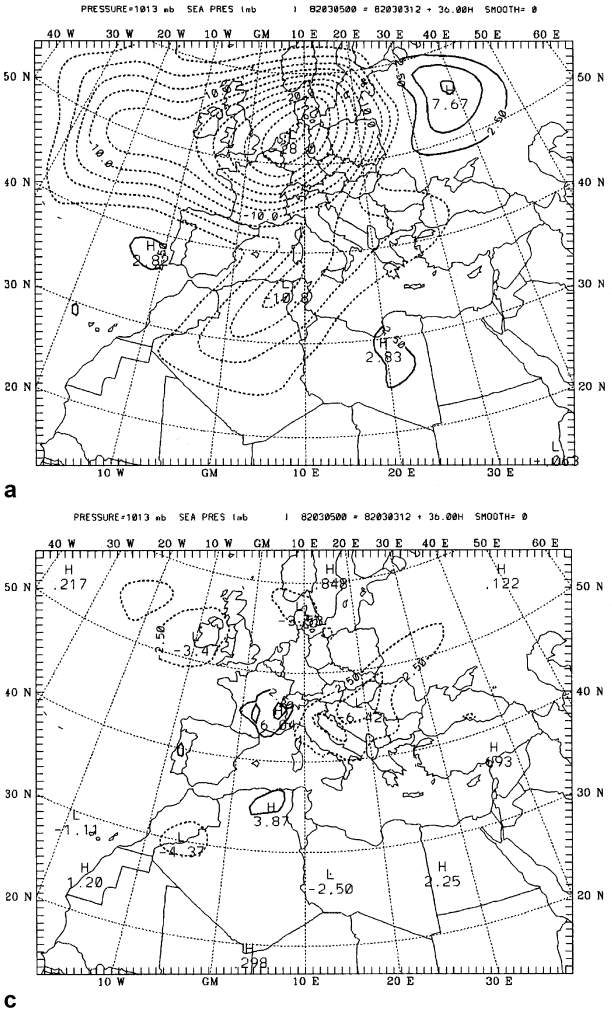

Fig. 19. As Fig. 18, but for 36 hours of simulation (5 March 00 GMT)

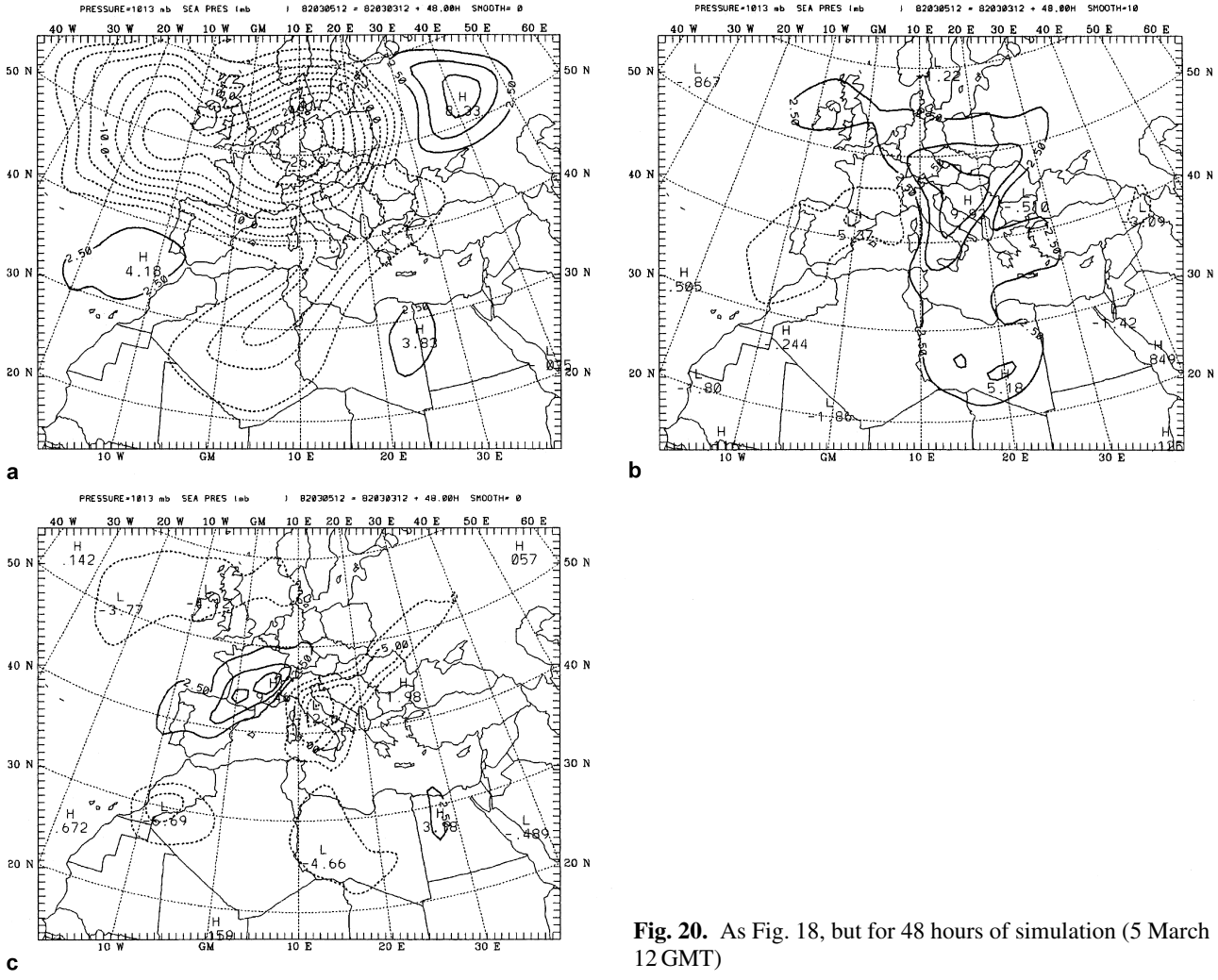

Fig. 20. As Fig. 18, but for 48 hours of simulation (5 March 12 GMT)

At 24 hours (Fig. 18) the dominant contributor to the pressure fall is the PV advection – about 13 hPa. The location of maximum PV influence is close to the actual position of the low. The pure topography has a much smaller deepening contribution of about 4 hPa to the south of the Alps with a more evident "anticyclonic" contribution to the north of the Alps. The maximum of "cyclonic" pure topography effect is to the west of the actual deepening (Fig. 18b). While both "pure PV" and "pure topography" affect the area to the southwest of the Alps, their synergic contribution has a rather different structure. It raises the pressure to the west of the Alps and drops it to the east of the Alps (Fig. 18c). The values for this synergic contribution are comparable to the topography contributions.

At 36 hours (Fig. 19) the maximum pure PV contribution in the lee moves further south and south to the Alps it has a significant value of about 10 hPa. The pure topography pattern becomes more elongated and still is primarily confined to the anticyclonic part. The synergic pattern turns slightly in clockwise direction, and its contribution *increases* both to the north and south of the Alps. The main contributor to the south of the Alps at the location of the low center ($\sim 12^\circ$ E, 45° N) remains the PV advection (about -10 hPa), the second contributor is the synergism between PV and topography (~ -5 hPa) while the mountains play a negligible or even slightly cyclolytic role (Fig. 19b).

It is surprising to see that at 48 hours (Fig. 20) the synergic effect quickly turns to be the number one contributor (13 hPa) and its pattern orientation resembles very much the 'classical' dipole structure of lee cyclones (e.g., Tibaldi et al., 1990). The pure PV contribution does not vary much from 36 hours while the pure topography contribution becomes entirely cyclolytic (~ 7 hPa)

at the location of the actual (as well as the control) low. The term "cyclolytic" here and later means opposite to cyclogenetic, i.e. contributing to the cyclone's filling. At this time, the pure topographical contribution remains cyclogenetic only much further to the west of the Alps.

Figures 18–20 show that the pure PV cyclogenetic effect is relatively large and does not vary much during the simulation. The pure topography effect produces a dipole structure oriented southwest – northeast at 24 hours and the dipole rotates slowly clockwise during the simulation. Its anticyclonic part is more evident than the cyclonic one. The synergic effect also reveals a dipole structure; at 24 hours it is oriented in east-west direction and then turns clockwise. The synergic contribution increases with time and at the maximum deepening it becomes the dominant one.

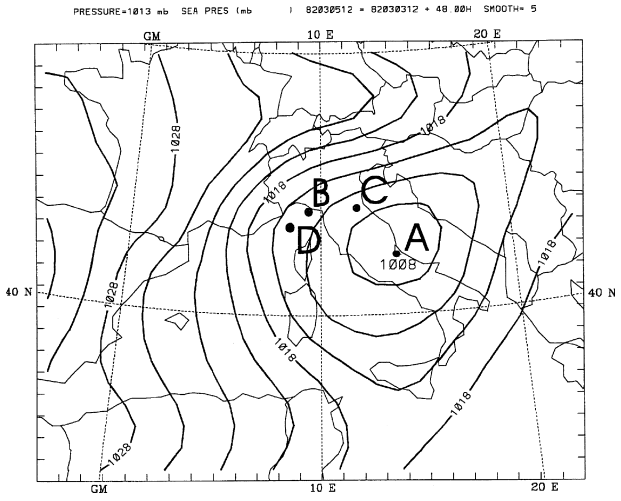

Fig. 21. Locations for the time series shown on Fig. 22. Background is sea-level pressure at 48 hours of simulation (5 March 12 GMT)

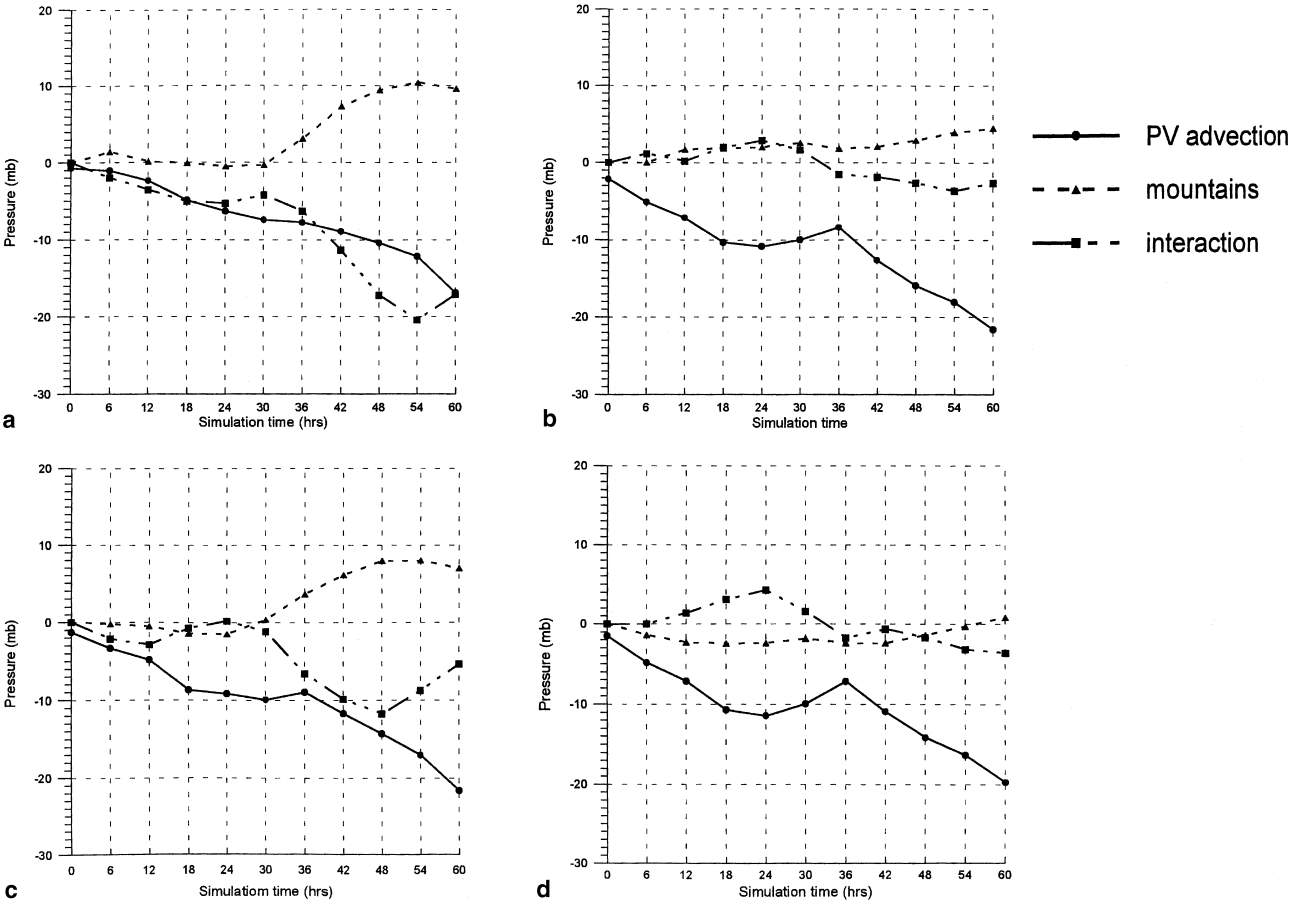

Fig. 22. The factor separated contributions to sea-level pressure of PV advection (circles), topography (triangles) and interaction (squares). The four time series for the points A, B, C and D indicated on Fig. 21 are shown

4.2 Time evolution of the factor-separated contributions

For the investigation of the time evolution of pure and synergic contributions during the simulation, several key geographical positions over the lee cyclogenetic region were chosen. The key points are shown in Fig. 21. Point A represents maximum deepening of the cyclone at 48 hours, points B and C correspond to the maximum deepening at 24 and 36 hours. Point D is located not far from the cyclone's center at 24 hours and it is under the ''cyclogenetic'' influence of the pure topography (Fig. 18b). Figure 22 illustrates that the major contributor at points B, C, D is PV advection. The interaction of PV advection with the mountains is very important at all points but plays a different role at various points. The most evident role is at point A; during the second stage of development – between 36 and 54 hours – the interaction becomes the primary contributor. At the points closer to the mountains (B, C, D) during the trigger phase – between 24 and 36 hours – the synergic cyclogenetic influence increases while the pure PV advection remains the major contributor, but its influence stabilizes and even decreases somewhat. At point C the interaction increases from zero to about 7 hPa, and together with pure PV advection it provides the maximum deepening at 36 hours despite the fact that the pure topography effect at this point becomes cyclolytic at about 4 hPa. It is interesting that the pure mountain cyclogenetic (but not the cyclolytic!) effect is very small at all points, even at the most western point D.

5. Discussion

From the spatial variation of the factor-separated contributors the following conclusions are derived. First, ''topography only'' produces its own dipole pattern that is in agreement with lee cyclogenesis theories (e.g., Speranza et al., 1985), when the flow interacts with a finite-length obstacle. The location of this dipole, however, is far from the dipole produced by the real cyclone. The interaction between advected PV and mountains also produces a dipole structure but its orientation depends mainly on the direction of the jet (or PV) propagation. During the ''trigger phase'' at 24–36 hours the synergic effect in the lee – at the actual cyclone's location – increases from zero to 3–5 hPa, and the pure topography effect is still cyclogenetic there during this time, while there is also a maximum contribution from pure PV advection. So, all factors contribute in cyclogenetic direction at the early stage. The synergic contribution, as well as the pure PV contribution, remains cyclogenetic up to the time of maximum deepening and the synergic effect even increases, but topography itself turns into a cyclolytic factor. Its cyclogenetic contribution at this later stage is only in an area that is far to the west of the observed cyclone.

It should be mentioned here that since the initial sea level pressure in ''PV−'' simulations is not exactly the same as in the ''PV+'' simulations (since it is affected by the PV modification in the upper troposphere), all quantitative results of the upper PV contribution contain also the initial low-level pressure differences which are a direct consequence of the PV reduction. Thus, when we say ''PV influence'' we really refer to both the upper level PV advection and to the downstream effect of the initial upstream differences in the surface pressure field.

The actual position and deepening of the control cyclone is found to result from a superposition of the four contributions, and the separation sheds light on the stages/processes of lee cyclogenesis. The ''trigger phase'' could be explained as a result of joint cyclogenetic actions of pure and synergic contributors during some period of time, their 'phase-locking' at some particular place. All three structures, obviously, are strongly dependent on the direction and intensity of the PV advection. Hence, relatively slight changes in the patterns' positions may result in ''unlocking'', and, consequently, in a rather quite different development. This could explain why lee cyclogenesis is not a ''robust'' phenomenon but very sensitive to the phasing of the different factors, and similar synoptic situations do not necessarily develop into a lee cyclone.

From the analysis of the time evolution of the factor-separated contributors the following picture emerges: At the beginning, before the trigger phase (0–24 hours), PV advection plays the major role, and its influence gradually increases. During the trigger phase its contribution

remains the primary one, and it is steady while the synergic term quickly increases to values almost equal to those due to the PV advection. During this period the pure mountain contribution remains small and could be even cyclolytic depending on the exact position of the point being analyzed. During the second stage, the pure topography effect turns to be strongly cyclolytic, and it partly even cancels the still increasing cyclogenetic effects of both PV advection and the synergic terms. At the final stage, the synergic term decreases, and its weakening allows the pure topographic cyclolytic contribution to fill the cyclone.

The experiments performed by Mattocks and Bleck (1986) with two factors switched on/off – mountains and upper-level PV – are quite similar to our simulations but for the idealized initial conditions and without employing a factor separation technique. Qualitative pictures in three of their simulations (they do not simulate the case with both factors switched off required for a full factor separation) are in a good agreement with our real-data runs.

In the study of Zupanski and McGinley (1989) the 3–6 March case is investigated along with a few other ALPEX cases. Three factors were chosen by the authors – low-level baroclinicity, upper-level jet and mountains – but, again, only on/off sensitivity studies were carried out for each factor without evaluation of any synergic effect. Hence, both their ''mountain'' and ''jet'' contributions actually contain also an interactive term that has not been isolated.

Egger (1995) suggested that in the area of the surface front the cold air in the lower layer might

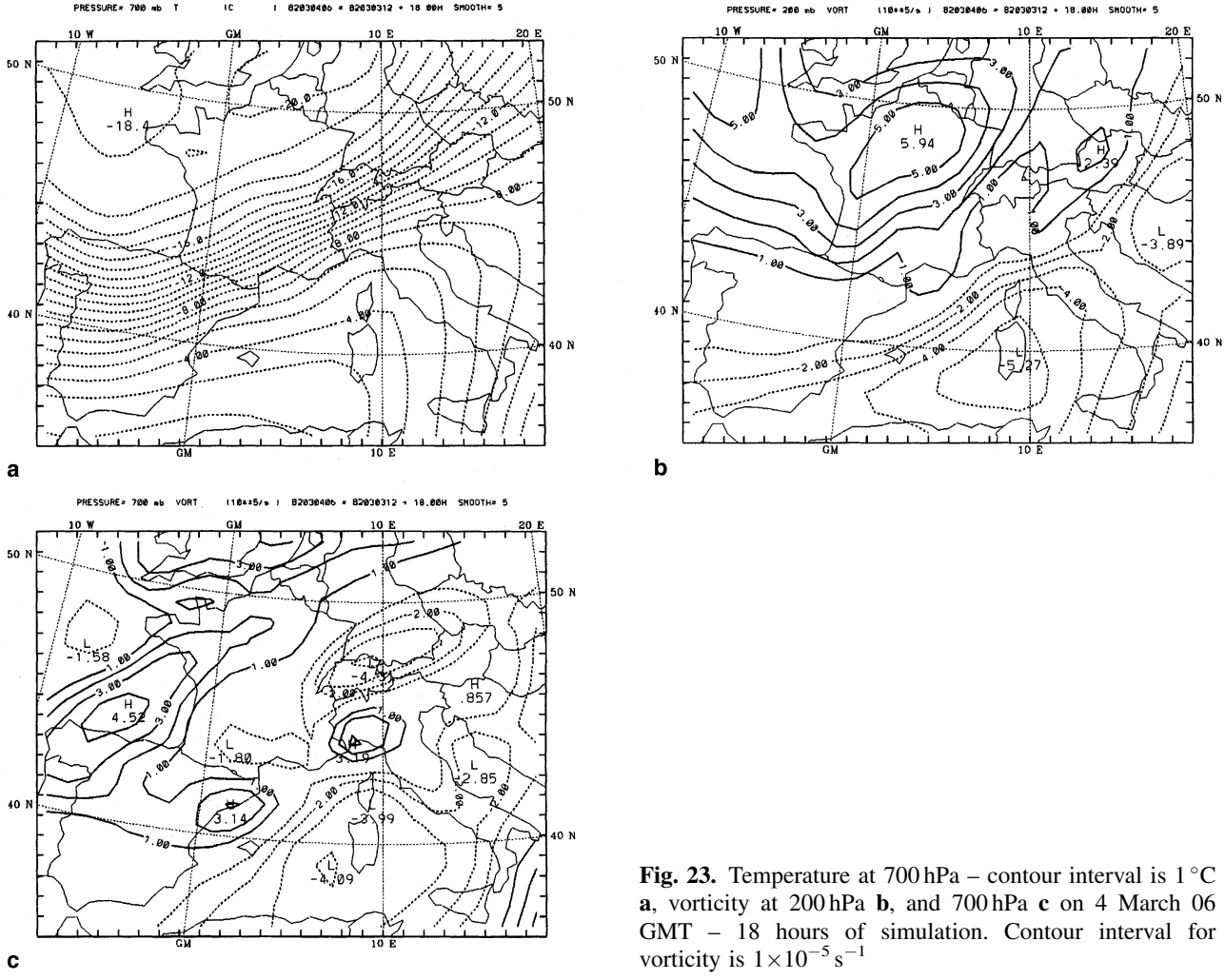

Fig. 23. Temperature at 700 hPa – contour interval is 1 °C **a**, vorticity at 200 hPa **b**, and 700 hPa **c** on 4 March 06 GMT – 18 hours of simulation. Contour interval for vorticity is $1\times10^{-5}\,s^{-1}$

mask the impact of the PV maximum above the front. While the mountains retard the cold air, the PV maximum is moving ahead and this allows the surface cyclone to be established in the lee. This suggestion seems to be in agreement with Mattocks and Bleck (1986) and with our simulations: Fig. 23 shows the area of the advancing surface front (Fig. 23a) and vorticity at upper and lower levels, Fig. 23b, c respectively. While the front is moving towards the mountains, the circulation in the upper layer is cyclonic (Fig. 23b) and in the low layer it is anticyclonic (Fig. 23c).

6. Conclusion

Simulations with the PSU/NCAR mesoscale model (MM5) were carried out in order to investigate the roles of topography and upper-level dynamics during lee cyclogenesis. The well-studied ALPEX case of 3–6 March 1982 was chosen for these experiments.

The factor separation method was applied to the dynamics of the process. Earlier, because of difficulties in switching off some dynamics elements in numerical models, mainly diabatic processes were chosen as factors. Here, the upper-level PV and topography were chosen as factors for the first time, and their pure and synergic contributions to the lee cyclogenesis were calculated for a better understanding of the Genoa cyclone generation mechanism.

The separation of topography and upper-level PV advection yields the following results regarding the sea-level pressure fall in the lee of the Alps:

(i) The pure contribution of PV advection is cyclogenetic during all times of simulation, and over the larger mountain area.

(ii) The pure topography contribution, in agreement with theories, produces a dipole structure, but the simulated pressure drops are relatively small compared to observations, and the dipole is oriented in a quite different direction, i.e. SW-NE. This northeast-southwest orientation is similar to that obtained by Zupanski and McGinley (1989) in their simulation without a jet. Also, the associated pressure fall is farther west from the actual location of the cyclone. At the point of maximum deepening in the lee of the Alps the pure topography contribution is very small in the pre-deepening and during the ''trigger'' phases, and even becomes strongly cyclolytic during later stages of cyclogenesis.

(iii) The synergic PV-topographic contribution is strong; during the later stages of the simulation it becomes comparable to the pure PV contribution and remains cyclogenetic during the full period of simulation. *This is the factor responsible for the dipole structure oriented in agreement with the observed picture*, *i.e. northwest-southeast*.

(iv) All factors as well as their interactions produce their own unique pattern of pressure changes. Their superposition, or ''locking'' in one place with joint cyclogenetic contributions clearly explains the rapid pressure fall during the ''trigger'' phase.

(v) Slight modifications in either the direction or the intensity of the PV advection may result in an 'unlocking' and a complete elimination of the joint contribution; this may result in a cyclone formation at some different location, or no cyclone at all. This seems to explain why lee cyclogenesis is highly sensitive to the synoptic conditions and why seemingly favorable conditions do not necessarily develop into a lee cyclone, as mentioned by e.g. Buzzi (1986), Orlanski and Gross (1994).

It seems to us that the strong synergic interaction found in the present study illustrates the significant nonlinearity of the cyclogenetic process. But, the method cannot explain the mechanism behind such amplification besides pointing to the conceptual model of Mattocks and Bleck (1986).

Acknowledgments

We wish to thank J. Egger for valuable comments. This research was supported by BSF grant No. 92-00275. This work has been also supported by the German Israel Foundation (GIF). Thanks to A. Tafferner for the help with the PV inversion program.

References

Alpert P, Tsidulko M (1994) Project WIND numerical simulations with the Tel-Aviv model: PSU-NCAR model run at Tel-Aviv University. Mesoscale Modelling of the Atmosphere (Pielke and Pearce, eds.) Meteorological Monographs V. 25, AMS, Boston, pp 81–95

Alpert P, Tsidulko M, Stein U (1995a) Can sensitivity studies yield absolute comparisons for the effects of several processes? J Atmos Sci 52: 597–601

Alpert P, Stein U, Tsidulko M (1995b) Role of sea fluxes and topography in eastern Mediterranean cyclogenesis. The Global Atmosphere-Ocean System 3: 55–79

Alpert P, Tsidulko M, Krichak SO, Stein U (1995c) A multistage evolution of an ALPEX cyclone. Tellus 48A: 209–220

Alpert P, Krichak SO, Krishnamurti TN, Stein U, Tsidulko M (1996) The relative roles of lateral boundaries, initial conditions and topography in mesoscale simulations of lee cyclogenesis. J Appl Meteorol 35: 1091–1099

Arakawa A, Lamb VR (1977) Computational design of the basic dynamical process of the UCLA general circulation model. Meth Comp Phys 17: 173–265

Black RX, Dole RM (1993) The dynamics of large-scale cyclogenesis over the North Pacific Ocean. J Atmos Sci 50: 421–442

Bleck R (1974) Short-range prediction in isentropic coordinates with filtered and unfiltered numerical models. Mon Wea Rev 102: 813–829

Bleck R, Mattocks C (1984) A preliminary analysis of the role of potential vorticity in Alpine lee cyclogenesis. Beitr Phys Atmos 57: 357–368

Buzzi A (1986) Review of the weather phenomena observed during the ALPEX special observing period. Sci Conf on the Results of the Alpine Experiment, Venice, 1985. WMO, Geneva, pp 15–27

Buzzi A, Trevisan A, Tosi E (1985) Isentropic analysis of a case of Alpine cyclogenesis. Beitr Phys Atmos 58: 273–284

Buzzi A, Trevisan A, Tibaldi S, Tosi E (1987) A unified theory of orographic influences upon cyclogenesis. Meteorol Atmos Phys 36: 1–107

Charney JG (1955) The use of primitive equations of motion in numerical prediction. Tellus 7: 22–26

Davis CA, Emanuel KA (1991) Potential vorticity diagnostics of cyclogenesis. Mon Wea Rev 119: 1929–1953

Dell'Osso L (1984) High-resolution experiments with the ECMWF model: a case study. Mon Wea Rev 112: 1853–1883

Egger J (1995) Interaction of cold-air blocking and upper-level potential vorticity anomalies during lee cyclogenesis. Tellus 47A: 597–604

Grell GA, Dudhia J, Stauffer DR (1993) A description of the fifth-generation Penn State/NCAR mesoscale model (MM5). NCAR Technical Note, NCAR/TN-398+STR, 117 pp

Hakim GJ, Keysler D, Bosart LF (1996) The Ohio Valley wave-merger cyclogenesis event of 25–26 January 1978. Part II: Diagnosis using quasigeostrophic potential vorticity inversion. Mon Wea Rev 124: 2176–2205

Haltiner G, Williams R (1980) Numerical prediction and dynamic meteorology. New York: Wiley, 477 pp

Henderson JM, Lackmann GM, Gyakum JR (1999) An analysis of hurricane Opal's forecast track errors using quasigeostrophic potential vorticity inversion. Mon Wea Rev 127: 292–307

Hoskins BJ, McIntyre ME, Robertson AW (1985) On the use and significance of isentropic potential vorticity maps. Quart J Roy Meteor Soc 111: 877–946

Huo Z, Zhang DL, Gyakum J (1998) An application of potential vorticity inversion to improving the numerical prediction of the March 1993 superstorm. Mon Wea Rev 126: 424–436

Huo Z, Zhang DL, Gyakum J (1999) Interaction of potential vorticity anomalies in extratropical cyclogenesis. Part I: Static piecewise inversion. Mon Wea Rev 127: 2546–2561

Huo Z, Zhang DL, Gyakum J (1999) Interaction of potential vorticity anomalies in extratropical cyclogenesis. Part II: Sensitivity to initial perturbations. Mon Wea Rev 127: 2563–2575

Khain AP, Rosenfeld D, Sednev I (1993) Coastal effects in the Eastern Mediterranean as seen from experiments using a cloud ensemble model with detailed description of warm and ice microphysical processes. Atmos Res 30: 295–319

Mattocks C, Bleck R (1986) Jet streaks dynamics and geostrophic adjustment processes during the initial stages of lee cyclogenesis. Mon Wea Rev 114: 2033–2056

McGinley JA, Zupanski M (1990) Numerical analysis of jets, fronts, and mountains on Alpine lee cyclogenesis: More cases from the ALPEX SOP. Meteorol Atmos Phys 43: 7–20

Orlanski I, Gross BD (1994) Orographic modification of cyclone development. J Atmos Sci 51: 589–611

Robinson WA (1988) Analysis of LIMS data by potential vorticity inversion. J Atmos Sci 45: 2319–2342

Speranza A, Buzzi A, Trevisan A, Malguzzi P (1985) A theory of deep cyclogenesis in the lee of the Alps. Part I: Modifications of baroclinic instability by localized topography. J Atmos Sci 42: 1521–1535

Stein U, Alpert P (1993) Factor separation in numerical simulations. J Atmos Sci 50: 2107–2115

Tafferner A, Egger J (1990) Test of theories of lee cyclogenesis. J Atmos Sci 47: 2417–2428

Tibaldi S, Buzzi A (1983) Effects of orography on Mediterranean lee cyclogenesis and its relationship to Europe blocking. Tellus 35A: 269–286

Tibaldi S, Buzzi A, Speranza A (1990) Orographic cyclogenesis. Extratropical Cyclones – The Eric Palmen Memorial Volume (Newton CW, Holopainen EO, eds.). Amer Meteorol Soc, pp 107–127

Tsidulko M (1998) A numerical investigation of synergistic contributions to lee cyclogenesis. Ph.D. Thesis, Tel Aviv University

Wu CC, Emanuel KA (1993) Interaction of a baroclinic vortex with background shear: Application to hurricane movement. J Atmos Sci 50: 62–76

Zupanski M, McGinley JA (1989) Numerical analysis of the influence of jets, fronts and mountains on Alpine lee cyclogenesis. Mon Wea Rev 117: 154–176

Authors' address: M. Tsidulko and P. Alpert, Department of Geophysics and Planetary Sciences, Tel Aviv University, Israel